Journal of Superconductivity, Vol. 11, No. 4, 1998

Temperature Dependence of Microwave Surface Impedance in High-T_c Single Crystals: Experimental and Theoretical Aspects

M. R. Trunin[1]

Received 10 May 1998

A systematic description of recent measurements of the real R_s and imaginary X_s parts of the microwave surface impedance $R_s + iX_s$ in high-quality high-T_c superconducting single crystals, namely $YBa_2Cu_3O_{6.95}$, $Ba_{0.6}K_{0.4}BiO_3$, $Tl_2Ba_2CaCu_2O_{8-\delta}$, $Tl_2Ba_2CuO_{6+\delta}$, and $Bi_2Sr_2CaCu_2O_8$, is given. Electrodynamic principles of experimental techniques and uncontrollable factors that affect the accuracy of $R_s(T)$ and $X_s(T)$ measurements are analyzed. Common and distinctive features in the temperature dependences of the surface impedance and complex conductivity in various high-T_c crystals are discussed. The experimental data are interpreted in terms of the two-fluid model taking into account scattering of quasiparticles and characteristic changes in the density of superconducting carriers as a function of temperature. The existing microscopic models of the microwave response of high-T_c superconductors are considered and prospects for further research are outlined.

KEY WORDS: Microwave response; surface impedance; complex conductivity; high-T_c single crystals; phenomenological models; microscopic theory.

1. INTRODUCTION

Measurements of the surface impedance of high-T_c superconductors (HTS) as a function of temperature, $Z_s(T) = R_s(T) + iX_s(T)$, yield information about the nature of quasiparticles in the superconducting state, their scattering, density of states, and, if a more sophisticated analysis is undertaken, about the superconducting pairing mechanism in these materials.

The real part of the surface impedance, i.e., the surface resistance R_s, is proportional to the loss of the microwave power and is caused by the presence of normal carriers. In the centimeter band of electromagnetic waves, typical values of the surface resistance of high-T_c single crystals in the normal state near the critical temperature T_c range between 0.1 and 0.4 Ω. At the point of the superconducting transition, the surface resistance abruptly drops, but it never turns to zero even when $T \to 0$. The residual surface resistance, $R_{res} \equiv R_s(T \to 0)$, is due to the presence of various defects in the superconductor surface layer. Given this fact, which was derived from experiments with conventional superconductors, it is generally accepted that the lower the R_{res}, the higher the sample quality. In this review we will consider measurements of stoichiometrically perfect single crystals of $YBa_2Cu_3O_{6.95}$ (YBCO), $Bi_2Sr_2CaCu_2O_8$ (BSCCO), $Tl_2Ba_2CaCu_2O_{8-\delta}$ (TBCCO), $Tl_2Ba_2CuO_{6+\delta}$ (TBCO), and $Ba_{0.6}K_{0.4}BiO_3$ (BKBO) whose doping level corresponds to the highest T_c, the superconducting transition width ΔT derived from measurements of $R_s(T)$ is small, $\Delta T \lesssim 1$ K, and R_{res} at frequency $f \sim 10$ GHz is within several milliohms. There is every reason to suppose that the electrodynamic parameters of these samples adequately characterize the intrinsic microscopic properties of superconductors.

The imaginary part of the surface impedance, i.e., the surface reactance X_s, is largely determined by the response of superconducting carriers and characterizes the nondissipating energy stored in the

[1]Institute of Solid State Physics, Russian Academy of Sciences, 142432 Chernogolovka, Moscow District, Russia.

0896-1107/98/0800-0381$15.00/0

superconductor surface layer. In the International System of Units SI, $X_s(T) \simeq \omega\mu_0\lambda(T)$ for $T < T_c$, where $\omega = 2\pi f$, $\mu_0 = 4\pi \cdot 10^{-7}$ H/m, and $\lambda(T)$ is the magnetic field penetration depth.

One can derive a superconductor's complex conductivity $\sigma_s = \sigma_1 - i\sigma_2$ from measurements of R_s and X_s. The functional relationship between Z_s and σ_s depends on the relation among three characteristic lengths, namely the mean free path l, the coherence length $\xi_0 = \hbar v_F / \pi\Delta(0)$, where v_F is the Fermi velocity and $\Delta(0)$ is the superconducting gap at $T = 0$, and λ. According to Abrikosov's concept [1], superconductors are classified as pure ($l > \xi_0$) and dirty ($l < \xi_0$) on the one hand, and London ($\xi \ll \lambda$) and Pippard ($\xi \gg \lambda$) on the other. As $T \to 0$, $\xi = \xi_0 \ll \lambda = \lambda_L \equiv (m/\mu_0 n e^2)^{1/2}$ in pure London superconductors and $\xi(l) \sim (\xi_0 l)^{1/2} \ll \lambda(l) \sim \lambda_L(\xi_0/l)^{1/2}$ in dirty superconductors. In pure Pippard superconductors $\xi = \xi_0 \gg \lambda \sim \lambda_L(\xi_0/\lambda_L)^{1/3}$, and in dirty superconductors $\xi(l) \gg \lambda(l)$. The relationship between the current and electric field in London superconductors is local (the London limit), whereas in Pippard superconductors this relation is essentially nonlocal (the Pippard limit). In accordance with these concepts, high-T_c materials should be classified with London superconductors, pure rather than dirty. In the case where the gap width is an anisotropic function of the electron quasimomentum, $\Delta(\vec{p})$, and has a line node on the Fermi surface of a pure superconductor, $\xi(\vec{p}) > \lambda_L$ in a narrow region about this line in the quasimomentum space. The contribution of this region to $Z_s(T)$ or $\sigma_s(T)$ should be expressed in terms of nonlocal electrodynamics, but theoretical estimates [2] indicate that nonlocal effects in this region are significant only at very low temperatures $T < 3$ K. Therefore, experimental data obtained at $T > 4.2$ K, which will be discussed in this review, can be interpreted using the simple local formula

$$Z_s = R_s + iX_s = \left(\frac{i\omega\mu_0}{\sigma_1 - i\sigma_2}\right)^{1/2} \qquad (1)$$

relating the surface impedance to the conductivity of HTS single crystals. Equation (1) allows us to express the real and imaginary parts of the conductivity in terms of the measurable quantities R_s and X_s:

$$\sigma_1 = \frac{2\omega\mu_0 R_s X_s}{(R_s^2 + X_s^2)^2}, \qquad \sigma_2 = \frac{\omega\mu_0(X_s^2 - R_s^2)}{(R_s^2 + X_s^2)^2} \qquad (2)$$

Above the superconducting transition temperature, the mean free path l of current carriers is shorter than the skin depth, $l \ll \delta$, which corresponds to the conditions of the normal skin effect. Equations (1) and (2) also apply to the normal state of HTS (at $T \geq T_c$), when $R_s(T) = X_s(T) = \sqrt{\omega\mu_0/2\sigma_n(T)}$ and $\sigma_n \equiv \sigma_1(T \geq T_c)$, $\sigma_2 = 0$.

An analysis of temperature dependences $Z_s(T)$ and $\sigma_s(T)$ allows one to check out whether this or that theoretical model provides an adequate description of electromagnetic properties of a superconductor.

In the low-frequency limit, $\hbar\omega \ll \Delta$, the Bardeen–Cooper–Schrieffer (BCS) theory [3] predicts two distinctive features in the T-dependence of the superconductor microwave response [3–5], namely an exponential drop in $\sigma_1(T)$ and $R_s(T) \propto \exp(-\Delta(0)/kT)$ in the range $T < 0.5T_c$, and an increase in the conductivity $\sigma_1(T)$ for $0.7 < T/T_c \leq 1$ with respect to its value σ_n at $T = T_c$. These features are due to the thermally activated generation of normal quasiparticles above the gap $\Delta(T)$ and the singularity in the density of states at a quasiparticle energy equal to $\Delta(T)$, respectively. The exponential section of $R_s(T)$ in conventional superconductors has been studied in detail (see, for example, [6] and references therein). On the other hand, the peak in $\sigma_1(T)$ in the region $T \sim 0.85T_c$ (the so-called coherent peak) was detected not so long ago in Nb and Pb at a frequency of 60 GHz [7] and in Nb at 10 GHz [8], when highly accurate concurrent measurements of $R_s(T)$ and $X_s(T)$ had become possible. Figure 1 shows as an example measurements of $R_s(T)$ and $X_s(T)$ of a niobium sample, whose critical temperature is $T_c = 9.2$ K. These measurements were obtained using the "hot finger" technique, which is convenient for studies of HTS crystals, whose surface area is usually small (~ 1 mm^2). The symbols ■ plot the function $\sigma_1(T)/\sigma_n$ derived from measurements of $R_s(T)$ and $X_s(T)$ using Eq. (2). These data are in agreement with calculations (solid curve) based on the BCS model.

The first measurements of functions $Z_s(T)$ and $\sigma_s(T)$ in HTS crystals did not show the behavior predicted by the BCS theory. In particular, instead of a broad coherent maximum in $\sigma_1(T)$ described by the BCS theory, a narrow peak (shown by the dashed line in Fig. 2) with a width close to that of the superconducting transition, which can be seen in the curve of $R_s(T)$, was observed. This observation indicated that strong-coupling (SC) effects should have been taken into account.

A generalized version of the BCS theory for the case of strong electron–phonon coupling was developed by Eliashberg [9]. It follows from this theory that, in the case of a strong enough coupling, the

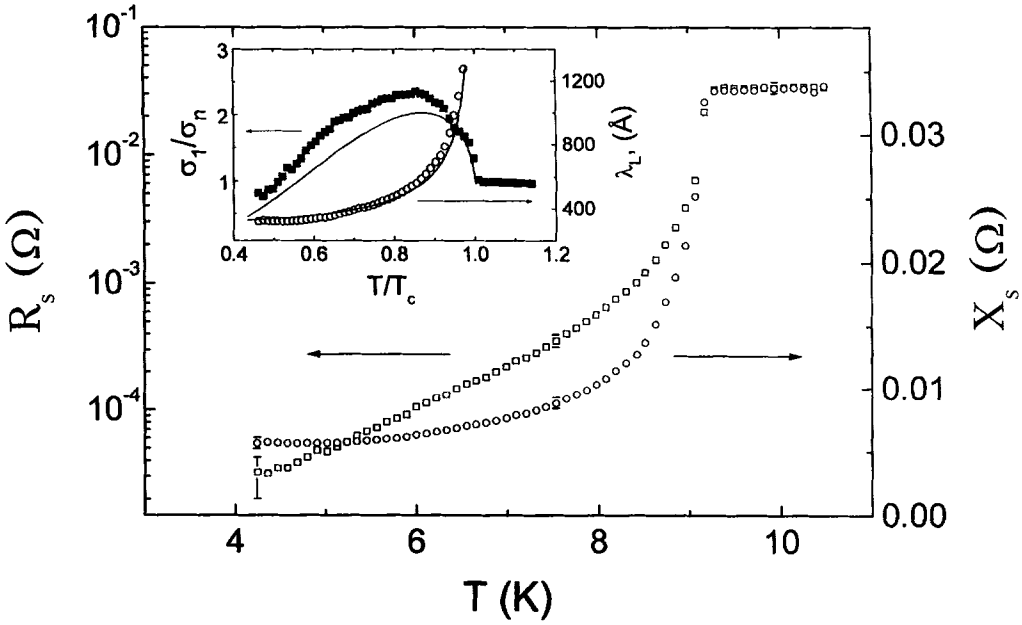

Fig. 1. Plots of $R_s(T)$ and $X_s(T)$ in Nb. The inset shows the real part of the conductivity, σ_1/σ_n, and the London field penetration depth, λ_L, vs. temperature derived from measurements of $R_s(T)$ and $X_s(T)$ using Eq. (2). The solid curves show calculations based on the BCS model.

singularity in the density of states at $\hbar\omega = \Delta(T)$ is broadened due to inelastic scattering of electrons by thermally excited phonons. As a result, the coherence peak amplitude decreases with an increase in the electron–phonon coupling constant and vanishes at frequencies around 10 GHz [10] if this constant is larger than 2. The inset to Fig. 2 shows curves of $\sigma_1(T)/\sigma_1(T_c)$ calculated on the base of the isotropic BCS and SC models. The narrow peak in Fig. 2, which is detected in microwave measurements of conductivity $\sigma_1(T)$ in HTS crystals around T_c, might be caused by inhomogeneous broadening of the superconducting transition [11,12] or fluctuation effects [13,14]. Another consequence of the SC model is the nonexponential behavior of $R_s(T)$ [15] and $\lambda(T)$ [16]. Power-law temperature dependences were also predicted by the well-known two-fluid Gorter–Casimir (GC) model [17], and near T_c they proved to be quite close to calculations by the SC model [18]. However, whereas the agreement between experimental curves on the one hand and calculations by the SC and GC models [18–20] on the other, in the neighborhood of T_c, could be deemed satisfactory, deviations in the low-temperature range were enormous. As an example, measurements of $\Delta\lambda_{ab}(T)$ in the *ab*-plane of YBCO given in [21] are compared with BCS and SC curves [22] in Fig. 3. A curve predicted by the GC phenomenological theory would be an almost horizontal straight line in this graph.

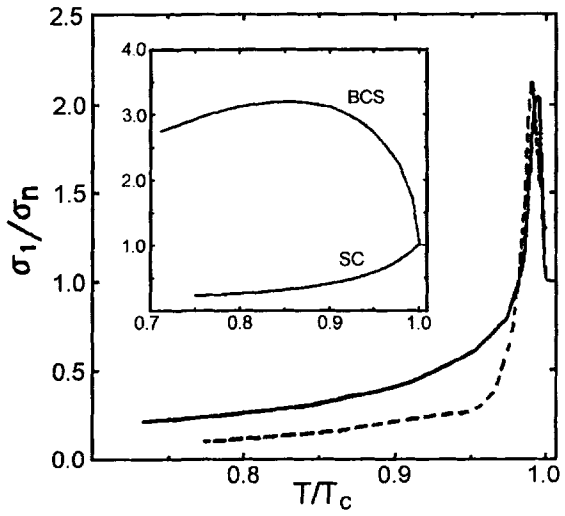

Fig. 2. Comparison between measurements (dashed line, YBCO crystal) of σ_1/σ_n and calculations based on the SC model taking into account inhomogeneous broadening of the superconducting transition (solid line). The inset shows σ_1/σ_n as a function of temperature calculated using the BCS and SC models [12].

The first high-quality YBCO crystals were manufactured at the University of British Columbia (UBC group) by Liang *et al.* [23]. A broad peak in the surface resistance vs. temperature, $R_s(T)$, centered at $T \approx 35$ K in those crystals was first reported by Bonn

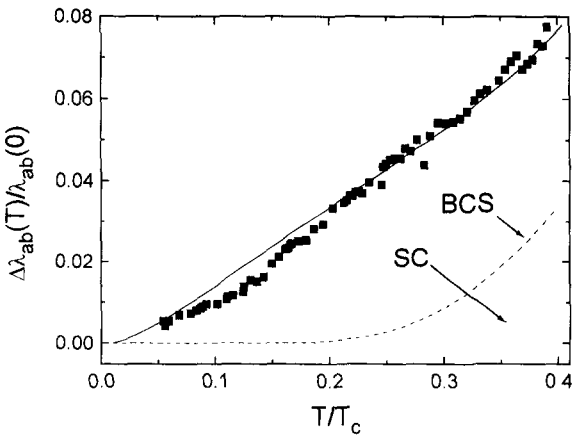

Fig. 3. Curves of $\Delta\lambda_{ab}(T)$ in the low-temperature range. The squares plot the data from [21]. The solid line shows calculations by the two-band model [22] (see Section 5). The dotted line is a calculation by the BCS model, the dashed line by the isotropic SC model.

et al. [24], and a linear dependence $\Delta\lambda_{ab}(T) \propto T$ in the range $4 < T \lesssim 25$ K by Hardy *et al.* [25].

These results, which seemed very unusual from the viewpoint of traditional models of the microwave response of superconductors, generated an intense discussion of the symmetry of the order parameter in HTS and the role of quasiparticle scattering, and stimulated development of theoretical models of the high-frequency response. By the present time, the first experimental data concerning YBCO single crystals [24,25] have been confirmed by experimenters from other laboratories. When high-quality BSCCO, BKBO, TBCCO, and TBCO single crystals had become available, it was possible to discuss common and distinctive features in the impedance and conductivity as functions of temperature of various HTS crystals.

The next section of the review is dedicated to the analysis of measurements that can be performed using the "hot finger" technique and its limitations, since this method is used in high-precision measurements of the HTS surface impedance vs. temperature in the microwave band more frequently than others. Section 3 describes systematized measurements obtained by means of this technique. Section 4 compares experimental curves of $Z_s(T)$ and $\sigma_s(T)$ to calculations based on the modified two-fluid model. In Section 5 we will discuss microscopic models that have been developed to this day and are based on possible symmetry types of the other parameter and mechanisms of quasiparticle relaxation. The concluding section describes prospects of further research in the microwave response of HTS single crystals.

2. EXPERIMENTAL PROCEDURE

2.1. Principles of the "Hot Finger" Technique

The most convenient technique for measurements of the surface impedance of small HTS samples is the so-called "hot finger" method. Measurements using this method in the centimeter wavelength band have been conducted at Northeastern University (NEU) [26], UBC, Maryland University [27], University of Tokyo [28], Cambridge University, University of California [29], and at the Institute of Solid State Physics (ISSP) [30]. The underlying idea of the method is that a sample is set on a sapphire rod at the center of a superconducting cylindrical cavity resonating at the H_{011} mode, i.e., at the antinode of a quasihomogeneous microwave magnetic field (Fig. 4). By varying the rod temperature, measuring the Q-factor and frequency shift Δf of the cylindrical cavity, and comparing them with the parameters of the empty cavity, Q_0 and Δf_0, one can determine the sample surface resistance R_s and reactance X_s as functions of temperature.

Electromagnetic modes driven by an external source are characterized in a lossy cavity by a complex frequency [31]

$$\hat{\omega}_i = \omega_i + i\omega_i/2Q_{iL} \tag{3}$$

where $\omega_i = 2\pi f_i$ and Q_{iL} are the inherent frequency and Q of the loaded cavity. For a cavity operated in

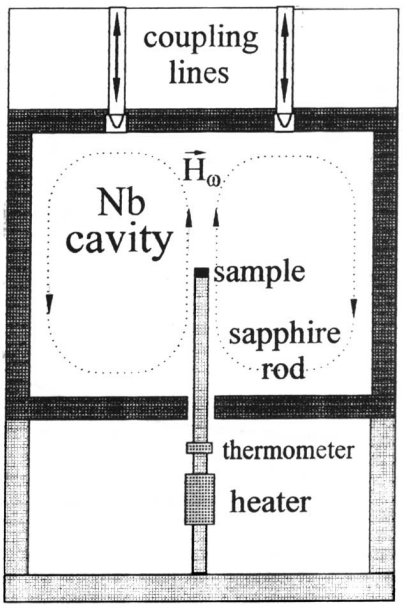

Fig. 4. Diagram of the microwave cavity used in the "hot-finger" technique.

the transmission mode

$$1/Q_{iL}=1/Q_i+1/Q_1+1/Q_2 \tag{4}$$

Here Q_i is the inherent Q of the unloaded cavity, and Q_1 and Q_2 are the input and output Q's, which characterize the coupling between the cavity and external microwave circuits. In Eqs. (3) and (4) $Q_{iL}=Q_L$, $Q_i=Q$, and $f_i=f$ if there is a sample in the cavity; $Q_{iL}=Q_{0L}$, $Q_i=Q_0$, and $f_i=f_0$ for the cavity without a sample but with a sapphire rod inside.

The difference between the averaged microwave powers absorbed in the cavity with a sample and the empty cavity is the power P directly absorbed in the sample:

$$P=\frac{1}{2}\int_S R_s H_s^2\, dS \tag{5}$$

where H_s is the tangential component of the microwave magnetic field on the sample surface, and integration is performed over the area S of the entire sample surface. The energy stored in the cavity is

$$W=\frac{\mu_0}{2}\int_V H^2\, dV \tag{6}$$

where V is the inside volume of the cavity, and H^2 is the magnetic field squared generated in the cavity with the sample inside. The difference between the reciprocal Q-factors of the cavity is determined by the relation

$$\frac{1}{Q}-\frac{1}{Q_0}=\frac{P}{\omega W}=\frac{R_s\int_S H_s^2\, dS}{\omega\mu_0\int_V H^2\, dV}=\frac{R_s}{\Gamma_s} \tag{7}$$

where

$$\Gamma_s=\frac{\omega\mu_0\int_V H^2\, dV}{\int_S H_s^2\, dS} \tag{8}$$

is the sample geometrical factor.

Let the complex resonant frequency of the loaded cavity be $\hat{\omega}$ and the frequency of the cavity without a sample be $\hat{\omega}_0$. The frequency difference $\hat{\omega}-\hat{\omega}_0$ is the frequency shift caused by the sample, $\hat{\omega}_s$. Provided that the coupling Q-factors Q_1 and Q_2 are constant, we derive from Eqs. (3), (4), and (7) the value of $\hat{\omega}_s$:

$$\hat{\omega}_s=\omega_s+\frac{i\omega R_s}{2\Gamma_s} \tag{9}$$

A change in the sample temperature leading to a change in its impedance, $\Delta Z_s(T)=\Delta R_s(T)+i\Delta X_s(T)$, can be treated as a small perturbation resulting in the shift $\Delta\hat{\omega}_s(T)$ in the complex frequency $\hat{\omega}=\hat{\omega}(Z_s)$:

$$\Delta\hat{\omega}_s(T)=\frac{\partial\hat{\omega}}{\partial Z_s}\Delta Z_s=\frac{\partial\hat{\omega}}{\partial Z_s}(\Delta R_s+i\Delta X_s) \tag{10}$$

On the other hand, as follows from Eq. (9),

$$\Delta\hat{\omega}_s(T)=\frac{i\omega}{2\Gamma_s}(\Delta R_s-2i\Gamma_s\Delta\omega_s(T)/\omega) \tag{11}$$

hence, by comparing this to Eq. (10), we obtain the change in the sample surface reactance

$$\Delta X_s(T)=-2\Gamma_s\Delta\omega_s(T)/\omega \tag{12}$$

where $\Delta\omega_s(T)=\Delta\omega(T)-\Delta\omega_0(T)$.

Thus, measurements of the real $R_s(T)$ and imaginary $X_s(T)$ parts of the surface impedance are derived from experimental curves of $Q_i(T)$ and $\Delta f_i(T)$ using the relations

$$\begin{aligned} R_s(T)&=\Gamma_s[Q^{-1}(T)-Q_0^{-1}(T)],\\ X_s(T)&=-\frac{2\Gamma_s}{f_0}[\Delta f(T)-\Delta f_0(T)]+X_0 \end{aligned} \tag{13}$$

where Γ_s is the sample geometrical factor given by Eq. (8) and X_0 is an additive constant.

As follows from Eq. (13), measurements of two quantities are needed to determine $R_s(T)$ and $X_s(T)$ in absolute units, namely X_0 and Γ_s. In measuring these quantities, one should take into account the strong anisotropy of layered HTS single crystals, which manifests in the notable difference between transport parameters in the *ab*-plane and along the *c*-axis. Therefore values of Γ_s and X_0, and the technique of their determination, depend on the crystal alignment (Fig. 5) with respect to the microwave magnetic field $\vec{H}_\omega$, which points along the cavity axis.

2.2. Samples, Their Geometrical Factors and Anisotropy

Let us start with the case of transverse orientation (Fig. 5a), when a sample, which usually has the shape of a plate with dimensions $a\sim b\sim 1$ mm, $c\sim 0.1$ mm, is set on an end of a sapphire rod so that the crystal *c*-axis is aligned with the microwave magnetic field, $\vec{H}_\omega$, $\vec{H}_\omega\parallel\vec{c}$. In this case, high-frequency currents, which determine the sample microwave response in both normal and superconducting states, circulate in the *ab*-planes. At $T<0.9T_c$ the field $\vec{H}_\omega$ penetrates into the sample to a depth $\lambda_{ab}\sim 10^{-4}$ mm, and at $T\geq T_c$ to the skin depth $\delta_{ab}=\sqrt{2\rho_{ab}/\omega\mu_0}$, which is $\delta_{ab}\sim 5\cdot 10^{-3}$ mm at a frequency of $\sim$10 GHz and the resistivity

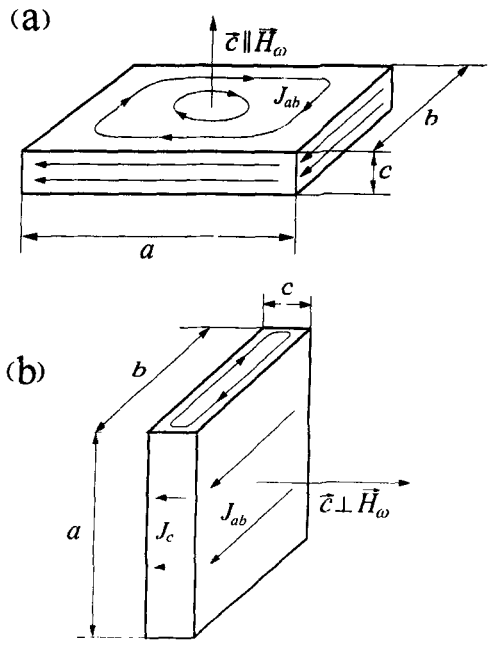

Fig. 5. (a) Transverse orientation of a sample with respect to microwave magnetic field, $\vec{H}_\omega \| \vec{c}$; arrows on the surfaces show directions of microwave currents; (b) transverse orientation, $\vec{H}_\omega \perp \vec{c}$.

$\rho_{ab}(T_c) \sim 100\ \mu\Omega \cdot$ cm typical of HTS crystals. Since $\lambda_{ab} \ll c$ and $\delta_{ab} \ll c$, then, neglecting the anisotropy in the ab-plane, it is possible

(1) to treat the impedance Z_s^{ab} as a parameter defined similarly to the case of a semi-infinite isotropic sample at all temperatures;

(2) to consider the distribution of the field H_s, hence the parameter Γ_s in Eq. (8), to be approximately constant with temperature.

For all HTS single crystals the inequality $\delta \gg l$, which is equivalent to the criterion of the normal skin effect, holds. For this reason, the constant X_0 in Eq. (13) for $\vec{H}_\omega \| \vec{c}$ is derived from the condition of equality between the real and imaginary parts of the normal state impedance, and the identity of the temperature dependences $R_s^{ab}(T)$ and $X_s^{ab}(T)$ in the range $T \geq T_c$ provides a simple test of the measuring technique.

Statements (1) and (2) give a clue to how the sample geometrical factor Γ_s^{ab} can be determined in the transverse orientation. Firstly, one can use a metallic simulator of the tested sample of the same shape and dimensions, provided that the conditions of the normal skin effect hold. Given the simulator resistivity as a function of temperature, $\rho(T)$, and having measured $Q_i(T)$ and $\Delta f_i(T)$ of the cavity containing the simulator, one can use the relation

$$\rho(T) = 2R_s^2(T)/\omega\mu_0 \tag{14}$$

and derive from Eq. (13) the value of Γ_s, assuming that it equals the geometrical factor Γ_s^{ab} of the HTS crystal. Secondly, having measured $Q_i(T)$ and $\Delta f_i(T)$ of the empty cavity and of the cavity loaded with the HTS crystal, one can directly measure $\rho_{ab}(T)$ of the sample and derive Γ_s^{ab} using Eqs. (13) and (14). This procedure, however, leads to degradation of a sample, because electric contacts should be attached to its surface. Nonetheless, we employed this technique in the determination of Γ_s^{ab} of two TBCCO and YBCO single crystals grown at ISSP using the techniques described in [32] and [33], respectively. Their dimensions were $a \times b \times c = 1 \times 1 \times 0.1$ mm^3 (TBCCO) and $1.5 \times 1.5 \times 0.1$ mm^3 (YBCO). In particular, the geometrical factor of the YBCO crystal proved to be $\Gamma_s^{ab} = 1.76 \cdot 10^4\ \Omega$.

We attempted to develop a method for estimating numerically the geometrical factor based on Eq. (8), assuming that a sample has the shape of a square plate with dimensions $a \times a \times c$, $c \ll a$, and the magnetic field amplitude at the center of the unperturbed cavity is H_0. The calculation procedure in which a flattened ellipsoid of revolution with semi-axes $c/2$ and $a/2$, on whose surface the field distribution is well known [34–36], was substituted for a square plate with the aim of determining Γ_s proved to be inadequate because the field amplitude on the ellipsoid edge, $H_{\text{edge}} = 2\pi a H_0/c$, is considerably higher than the real value. A more realistic model considers the sample as a thin plate with slightly rounded edges [37]. This approach yields the well-known geometrical barrier to penetration of flux lines from the sample edges [37–39]. In this case, the field distribution on the edges of a plate in the Meissner state is given by the formula [37] $H_s(x) = H_0 x/\sqrt{(a/2)^2 - x^2}$, $-a/2 + c/4 \leq x \leq a/2 - c/4$, with the exception of a very narrow region ($\approx c/4$) near the edge, where the integral $\int_S H_s^2\, dS$ is logarithmically divergent. On the edges of the sample, the field is assumed to be homogeneous and equal to $H_{\text{edge}} \approx H_0\sqrt{a/c}$. As a result, we have at $c \ll a$

$$\int_S H_s^2\, dS = 16 \int_0^{(a-c/2)/2} H_s^2(x) x\, dx + 4acH_0^2 a/c$$

$$\simeq 2H_0^2 a^2 \left(\ln\left(\frac{a}{c}\right) + 1 \right) \tag{15}$$

By substituting Eq. (15) in (8), we obtain the geometrical factor of HTS crystals for the case of their

transverse alignment with respect to the microwave field $\vec{H}_\omega$ in the cavity:

$$\Gamma_s = \frac{\omega\mu_0 V}{4\gamma_0 A}\left(\ln\left(\frac{a}{c}\right)+1\right)^{-1}, \qquad \gamma_0 = \frac{VH_0^2}{2\int_V H^2\,dV} \tag{16}$$

where A is the area of the ab-face of the crystal, and γ_0 is a constant determined by the known [40] field configuration of the resonant mode H_{011}. In the cavity used in our experiments, whose diameter and height were 42 mm ($f=9.4$ GHz), this constant $\gamma_0=5.3$. The calculations of Γ_s by Eq. (16) for YBCO and TBCCO crystals were in satisfactory agreement with experimental data. Figure 6 shows as an example measurements of $R_s(T)$ and $X_s(T)$ in a YBCO sample ($\Gamma_s = 1.76\cdot 10^4\ \Omega$), which demonstrate the behavior typical of the HTS single crystal impedance for $\vec{H}_\omega \parallel \vec{c}$. The uncertainty δR_s in measurements of the surface resistance, $\delta R_s = \Gamma_s \delta(Q^{-1}-Q_0^{-1}) = \Gamma_s \delta Q/Q^2$, is determined by the uncertainty $\delta Q/Q$, which was within 1% at $Q\sim 10^7$ in the reported experiments. Thus, we have $\delta R_s \approx 20\ \mu\Omega$. As the temperature drops several degrees below T_c, the increment $\Delta X_s(T) = \omega\mu_0\Delta\lambda(T)$, and, given $X_s(T)$ expressed in absolute units, one can determine the magnetic field penetration depth $\lambda(T)=X_s(T)/\omega\mu_0$. The uncertainty in the relative value of the penetration depth $\Delta\lambda(T)$, $\delta(\Delta\lambda)=(2\Gamma_s/\omega\mu_0)\cdot(\delta(\Delta\omega)/\omega)$, which equals several ångströms, and the error in $\lambda(T)$ can be up to 10% of $\lambda(0)$ and is largely determined by the accuracy of X_0.

Now let us consider an alternative crystal orientation with respect to the field $\vec{H}_\omega$ in the cavity, namely $\vec{H}_\omega \perp \vec{c}$ (Fig. 5b). Measurements of the surface impedance $Z_s^{\vec{H}_\omega \perp \vec{c}}(T)$ in this orientation, dubbed longitudinal, are interesting primarily because they yield

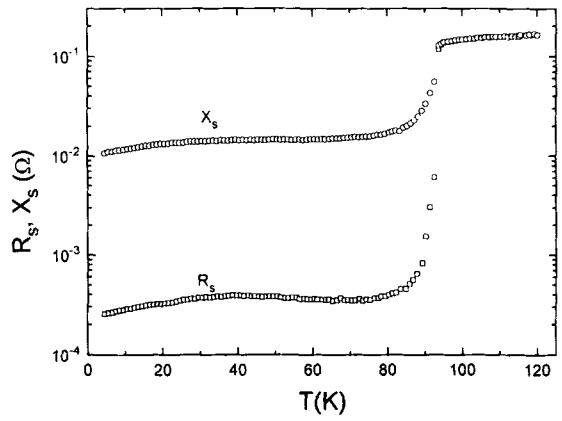

Fig. 6. Surface resistance R_s and reactance X_s of a YBCO single crystal as functions of temperature.

information about anisotropic properties of HTS crystals. Given that $\vec{H}_\omega \perp \vec{c}$, the tangential field component H_s on the edges of the sample can be considered to be approximately equal to H_0 ($H_s \approx H_0$). In the superconducting state, currents running in the ab-planes decay over a depth λ_{ab}, whereas those flowing in the direction of the c-axis have a penetration depth λ_c, and at $T<0.9T_c$ these two lengths are smaller than characteristic sample dimensions, which allows us to treat the impedance $Z_s^{\vec{H}_\omega \perp \vec{c}}$ in its conventional sense assuming a conductor occupying a half-space. At $T>0.9T_c$, however, the size effect may play an essential role [36]. Indeed, whereas the ratio $\delta_c/\delta_{ab}\sim 10$ in YBCO single crystals, and in the frequency band about 10 GHz $\delta_c \sim 0.05$ mm is comparable to the sample thickness c but less than a and b, in BSCCO, for example, this ratio can be up to 300, so that $\delta_c \sim a \sim b$. As a result, statements (1) and (2), which hold at all temperatures in the case of transverse orientation, no longer apply to the $\vec{H}_\omega \perp \vec{c}$ configuration at $T>0.9T_c$. Owing to the size effect, the functional dependence $\Delta R_{s,eff}^{\vec{H}_\omega \perp \vec{c}}(T)$ deviates from $\Delta X_{s,eff}^{\vec{H}_\omega \perp \vec{c}}(T)$ at $T>T_c$, which makes impossible determination of constant X_0 in Eq. (13) using the method described above, and the experimental measurement of the sample geometrical factor entails formidable difficulties.

There are no such difficulties at $T<0.9T_c$. If we neglect the anisotropy in the ab-plane (which is possible, for example, in the case of twinned YBCO crystals) and the contribution from bc-faces (Fig. 5b), which is a factor $\sim c/a$ smaller than that of the ab-surfaces, the impedance $Z_s^{\vec{H}_\omega \perp \vec{c}}$ is expressed in terms of $Z_s^{ab} = Z_s^{\vec{H}_\omega \parallel \vec{c}}$ and Z_s^c averaged over the surface area [41–43]:

$$Z_s^{\vec{H}_\omega \perp \vec{c}} \simeq \frac{abZ_s^{ab} + acZ_s^c}{ab+ac} = \frac{bZ_s^{ab} + cZ_s^c}{b+c} \tag{17}$$

where the superscripts (ab or c) of Z_s denote the direction of the screening current. The sample geometrical factor for $\vec{H}_\omega \perp \vec{c}$ is easily derived from Eq. (8), and the constant X_0 in Eq. (13) is determined by the condition $X_s^c(0)=\omega\mu_0\lambda_c(0)$ with $\lambda_c(0)$ derived independently from alternative experimental data. Given measurements of $Z_s^{ab}(T)$ in the transverse orientation and $Z_s^{\vec{H}_\omega \perp \vec{c}}(T)$ with the sample plane aligned with the field, one can obtain $R_s^c(T)$ and $\lambda_c(T)=X_s^c(T)/\omega\mu_0$ from Eq. (17).

There is an alternative technique for determination of $R_s^c(T)$ if one of the sample dimensions in the ab-plane, for example a, is notably larger than another: $a>b>c$. By measuring first the power

$P^{\vec{H}_\omega \| a}$ absorbed in the sample whose a-axis is aligned with the field $\vec{H}_\omega$, then $P^{\vec{H}_\omega \| b}$, we obtain

$$R_s^c \simeq \frac{P^{\vec{H}_\omega \| \vec{a}} - P^{\vec{H}_\omega \| \vec{b}}}{c(a-b)H_0^2} \tag{18}$$

In deducing Eq. (18), we have assumed that $R_s^a \approx R_s^b$. Zhang *et al.* [44] measured the *ab*-plane anisotropy of the microwave surface impedance of untwinned YBCO single crystals by performing measurements in configurations $\vec{H}_\omega \| \vec{a}$ and $\vec{H}_\omega \| \vec{b}$ under the assumption that

$$P^{\vec{H}_\omega \| \vec{a}} \simeq (abR_s^b + acR_s^c)H_0^2,$$
$$P^{\vec{H}_\omega \| \vec{b}} \simeq (abR_s^a + bcR_s^c)H_0^2 \tag{19}$$

A rough estimate of R_s^c in [44] yielded $\sim R_s^a$ ($\sim R_s^b$), which allowed the researchers to neglect the second terms on the right-hand sides in Eq. (19), as compared with the first terms, in the case of very thin crystals, $a \sim b \gg c$, and determine $R_s^a(T)$ and $R_s^b(T)$. In order to increase the c-axis contribution, an HTS crystal was cleaved [43,45], for example, into four bars along the a-axis, and the four samples obtained in this manner were tested in the configuration $\vec{H}_\omega \| \vec{a}$. By taking the difference between the curves of $P^{\vec{H}_\omega \| \vec{a}}(T)$ recorded before and after cleaving the sample, the experimenters derived $R_s^c(T)$, $R_s^b(T)$, and $R_s^a(T)$ in accordance with Eq. (19).

The feasibility proof of these techniques for measuring the anisotropy of HTS crystals in the longitudinal orientation, $\vec{H}_\omega \perp \vec{c}$, described above requires, in our opinion, a more substantial electrodynamic analysis. In particular, the field distribution on the sample surface and its geometrical factor can change considerably as a result of the transition to the superconducting state, which should affect measurements of $Z_s^{\vec{H}_\omega \perp \vec{c}}(T)$ around T_c. In deriving Eqs. (17)–(19) the contribution P_{bc} of the bc-faces of the crystal (Fig. 5b) to the total power absorbed by the sample, $P^{\vec{H}_\omega \perp \vec{c}} = P_{ab} + P_{ac} + P_{bc}$, has not been taken into account. This contribution is really small in comparison with P_{ab}, $P_{bc}/P_{ab} \sim c/a \ll 1$, but may be comparable to P_{ac}. For example, assuming a field distribution over the bc-face of the simplest form, $H_x = 2H_0 x/c$, $H_y = 2H_0 y/b$ $(-c/2 \le x \le c/2, \ -b/2 \le y \le b/2)$, we obtain directly an estimate of the ratio $P_{bc}/P_{ac} \sim b/a \sim 1$ for $\vec{H}_\omega \| \vec{a}$. Now, if the contribution P_{bc} is included in Eq. (19), it is clear that the comparison between $P^{\vec{H}_\omega \| \vec{a}}(T)$ and $P^{\vec{H}_\omega \| \vec{b}}(T)$ in the initial sample, on the one hand, and $P^{\vec{H}_\omega \| \vec{a}}(T)$ of its fragments produced by cleaving the crystal along the a-axis, on the other, yields, in the long run, the same result for R_s^c, but the quantities $R_s^b(T)$ and $R_s^a(T)$, previously determined neglecting P_{bc}, should change. The real field distribution over the sample surface in the longitudinal orientation can be calculated numerically. Finally, the sample alignment with respect to the microwave field, $\vec{H}_\omega \perp \vec{c}$, should be controlled carefully in performing measurements in this configuration. Deviations from the initial configuration, which may occur when the sample is replaced by its cleaved fragments or rotated around the c-axis, can give rise to uncontrolled errors in measurements. This or another circumstance may be the cause of contradictions among different measurements of Z_s^c in YBCO single crystals that have been published by this time [41,42,45]. For this reason, most of the material given in this review is dedicated to measurements of the microwave response of HTS crystals in the transverse orientation.

Let us also discuss impedance measurements of BKBO crystals, which are almost isotropic, absolutely copper-free, and have a cubic perovskite structure. They were manufactured by the electrochemical crystallization technique [46,47]. The studied BKBO samples had an approximately cubic shape and volumes in the range $0.2 \le V \le 1.5$ mm^3. The procedure for determining the geometrical factor was the following. The niobium sample simulator had approximately the same shape and dimensions as the tested sample. If the samples were of an elliptic shape, their geometrical factors Γ_{BKBO} or Γ_{Nb} could be calculated exactly. For example, the geometrical factor of a sample shaped as a sphere with radius r at the center of a cavity excited at the H_{011} mode is $\Gamma_s = \omega\mu_0 V / 12\pi\gamma_0 r^2$ [29]. Therefore our first step was estimating $\Gamma_{1,\text{Nb}}$ and $\Gamma_{1,\text{BKBO}}$ based on the assumption that the samples were spheroids with volumes equal to those of measured Nb and BKBO samples. The second step was based on the experimental technique used in determining Γ_{Nb}. We measured the resistivity ρ_{Nb} (10 K) of a thin Nb stripe cut from the same block as the niobium sample simulator, calculated the surface resistance R_s (10 K) using Eq. (14), and substituted the result in Eq. (13) alongside the measurements of $Q_{i,Nb}(T)$. The resulting Γ_{Nb} proved to be only 24% smaller than $\Gamma_{1,\text{Nb}}$ calculated on the first step. Given that the shapes of the Nb and BKBO samples were almost identical, we decided that the geometrical factor of BKBO samples $\Gamma_{\text{BKBO}} = 0.76 \cdot \Gamma_{1,\text{BKBO}}$. An example of experimental $R_s(T)$ and $X_s(T)$ curves of the BKBO crystal with geometrical factor $\Gamma_s = 3.3 \cdot 10^4\ \Omega$ is given in Fig. 7.

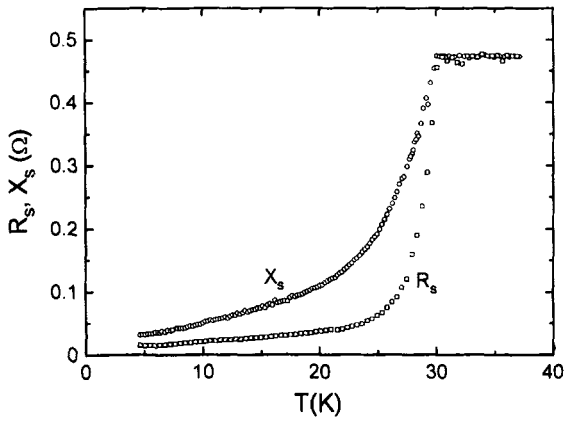

Fig. 7. Surface resistance R_s and reactance X_s of a BKBO single crystal vs. temperature.

2.3. Thermal Expansion of Crystals

There is a set of factors that affect the accuracy of measurements of Q and resonant frequency shift, hence absolute measurements of $R_s(T)$ and $X_s(T)$. They include:

—vacuum tightness of the microwave cavity;
—changes in the pressure applied to the cavity;
—reproducibility of positions of the sapphire rod and external coupling loops in the cavity with and without a sample;
—constancy of the liquid helium level in the cryostat in all experiments;
—stability of electronic circuits.

These factors are monitored in the course of the experiment; thus measurement uncertainties that may be caused by these factors can be minimized, if the necessary conditions are satisfied strictly.

The uncontrolled source of possible errors in measurements of $\lambda(T)$ is thermal expansion of the sample. Changes Δl_i (Δa and Δc) in the sample dimensions $a \times a \times c$, where $c \ll a$, due to the thermocycling lead to a change in its volume by $\Delta c \cdot a^2 + 2\Delta a \cdot ac$ and an additional shift of the cavity resonant frequency

$$\Delta f_l(T) = \frac{f_0 \mu_0}{4W} \int_S \Delta l_i(T) H_s^2 \, dS \qquad (20)$$

where W is given by Eq. (6). Strictly speaking, the quantity $\Delta f_l(T)$, alongside $\Delta f_0(T)$, should be included in Eq. (13) for $X_s(T)$. Let us estimate this contribution by comparing expression (20) with the resonant frequency shift due to the change in the field penetration depth $\Delta\lambda(T)$:

$$\Delta f_\lambda(T) = \frac{f_0 \mu_0}{4W} \int_S \Delta\lambda(T) H_s^2 \, dS \qquad (21)$$

If the *ab*-plane of the crystal is perpendicular to the magnetic field $\vec{H}_\omega$ (transverse orientation, Fig. 5a) in measurements of $\Delta\lambda_{ab}(T)$, then, using Eqs (15), (20), and (21), one can easily show that

$$\frac{\Delta f_l}{\Delta f_\lambda} = \frac{\Delta c/2(\ln(a/c) - 1) + \Delta a}{\Delta\lambda_{ab}(\ln(a/c) + 1)} \qquad (22)$$

In YBCO and BSCCO single crystals with $T_c \simeq 90$ K, λ_{ab} increases by about 1000 Å as the temperature grows from 4.2 to 80 K, and at $T > 80$ K the growth rate is considerably higher. Experimental data indicate that at $T < 30$ K the relative change in dimensions of YBCO [48–50] and BSCCO [51,52] crystals, $\varepsilon = \Delta l_i / l_i$, is very small, $\varepsilon_i < 10^{-5}$. In the temperature range $30 < T < 100$ K the thermal expansion coefficient $\alpha_i = d\varepsilon_i/dT$ is an almost linear function of temperature T; moreover, in the *ab*-plane of YBCO crystals $\alpha_{ab} \approx 0.3 \cdot 10^{-7} T$, and in the direction of the *c*-axis $\alpha_c \approx 10^{-7} T$. Hence we have $\varepsilon_{ab} \approx 10^{-4}$ and $\varepsilon_c \approx 3 \cdot 10^{-4}$, and for typical crystal dimensions $a \approx b \approx 1$ mm and $c \approx 0.1$ mm they increase by $\Delta a \approx \Delta b \approx 1000$ Å and $\Delta c \approx 300$ Å when the temperature grows from 30 to 100 K. In BSCCO single crystals ε_{ab} is twice as large, and ε_c is approximately the same as in YBCO. Relative changes in dimensions of BKBO crystals in the temperature interval $0 < T \leq 2T_c$ are very small, $\varepsilon < 10^{-5}$ [53]. To the best of our knowledge, no data on thermal expansion of TBCO and TBCCO for $T \leq T_c$ are available.

Thus, the contribution of $\Delta f_l(T)$ to the total frequency shift of a cavity loaded with a sample is negligible in the range of low temperatures. In the intermediate range, however, it can be quite considerable, although smaller than $\Delta f_\lambda(T)$, as follows from the estimate by Eq. (22). This circumstance should be taken into account when using Eq. (13) in the determination of $\lambda_{ab}(T)$. Since the thermal expansion of samples is not measured in microwave experiments, the only criterion of the authenticity of experimental curves of $\lambda_{ab}(T)$ is their reproducibility for crystals of different sizes. For example, let us compare curves of $\Delta\lambda_{exp}(T) \propto \Delta f_{exp}(T) = [\Delta f(T) - \Delta f_0(T)]$ measured in YBCO crystals of dimensions $a \approx b \approx 1.4$ mm, $c \approx 0.1$ mm [54] and $a \approx b \approx 1.5$ mm, $c \approx 0.1$ mm [33] with curves of $\Delta\lambda(T) \propto [\Delta f_{exp}(T) + \Delta f_l(T)]$ plotted

taking into account $\Delta f_l(T)$. In Fig. 8 the lower solid line 1 and dashed line 2 show the numerator on the right of Eq. (22) as a function of temperature for two YBCO crystals with dimensions a and c given in the caption. The measurements of $\Delta c(T) = c \int \alpha_c(T)\, dT$ and $\Delta a(T) = a/2 \int [\alpha_a(T) + \alpha_b(T)]\, dT$ are taken from [50]. The full symbols (λ_{exp}) in Fig. 8 plot experimental data quoted in [54] (1) and [33] (2), and the open symbols (λ) show the data processed using Eq. (22) and taking into account thermal expansion of the crystals. At $T < 50$ K the curves of $\lambda_{exp}(T)$ and $\lambda(T)$ coincide, whereas in the region of higher temperatures there is a difference between them.

Let us also estimate the factor $\Delta f_l(T)$ in the case if the ab-plane is parallel to the microwave field $\vec{H}_\omega$ (longitudinal orientation, Fig. 5b). In this case the experiment measures the effective parameter $\lambda_{eff}(T) = X_s^{\vec{H}_\omega \perp \vec{c}}(T)/\omega\mu_0$, related to $\lambda_{ab}(T)$ and $\lambda_c(T)$ by Eq. (17). For $c/a \ll 1$ we derive from Eqs. (20) and (21)

$$\frac{\Delta f_l}{\Delta f_\lambda} \simeq \frac{\Delta c(1 + \varepsilon_{ab}/\varepsilon_c)}{2\Delta\lambda_{eff}} \tag{23}$$

It follows from Eq. (23) that thermal expansion of crystals can lead to variations $\sim\Delta c$ in $\lambda_{eff}(T)$ measured in the configuration $\vec{H}_\omega \perp \vec{c}$.

3. MEASUREMENTS OF SURFACE IMPEDANCE AND COMPLEX CONDUCTIVITY OF YBCO, BSCCO, TBCCO, TBCO, AND BKBO CRYSTALS: THEIR COMMON AND DISTINCTIVE FEATURES

First measurements of the surface impedance of HTS materials in the microwave band date back to the time of their discovery in 1986–1987. The first microwave experiments with ceramic samples, as well as thin films and single crystals, which were fabricated soon after the discovery of HTS, were rare and produced only rough estimates of HTS parameters since the quality of those samples left much to be desired. In particular, the residual surface resistance $R_{res} = R_s(T \to 0)$ was several orders of magnitude higher than in conventional superconductors like Nb or Pb, and it was clear to everyone that high-frequency properties of HTS materials were largely determined by irregularities in their structures, namely their inhomogeneity and the presence of weak-coupling sites, twins, and other defects in their surface layers.

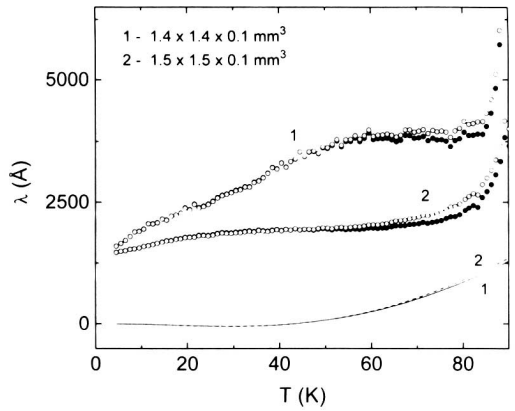

Fig. 8. Effect of sample thermal expansion on the penetration depth λ_{ab} plotted against temperature for two YBCO single crystals.

The situation changed radically in 1992–1993, when first high-quality YBCO single crystals [23–25] and thin films [55] with considerably smaller R_{res} were fabricated. Measurements of those samples revealed a temperature dependence of the surface impedance, $Z_s(T)$, which could not have been detected in earlier experiments against the background of high residual losses. The UBC group detected for the first time

(a) linear dependences $\lambda_{ab}(T)$ and $R_s(T)$ in the range $4 < T \lesssim 25$ K, and
(b) a broad peak in $R_s(T)$ centered at about 40 K.

These features of $Z_s(T)$ in YBCO single crystals were confirmed by experiments performed by other groups [33,41,42,56] and have been generally recognized by this time. We stress once again that features (a) and (b) can be observed only in YBCO crystals of the highest quality. Doping of initially perfect single crystals with Zn [57–59] changes the linear function $\lambda_{ab}(T)$ to quadratic and spreads the peak in $R_s(T)$. The dependence $\Delta\lambda_{ab}(T) \propto T^2$ is typical of YBCO thin films [60–62], in which impurities and weak coupling sites occur more frequently than in single crystals. Therefore it is generally accepted that the quadratic dependence $\lambda(T)$ is largely due to the presence of defects in samples (extrinsic origin), unlike features (a) and (b), which are due to intrinsic microscopic properties of HTS materials. This conjecture was later confirmed by systematic research of YBCO thin films [63]: As their quality improved, the quadratic dependence $\lambda(T)$ in the low-temperature range was replaced by a linear function. A detailed analysis of the results mentioned above and concerning microwave studies of YBCO crystals and films before 1996 is given in the review by Bonn and Hardy [64].

Given the apparent difference between the temperature dependences in YBCO and conventional

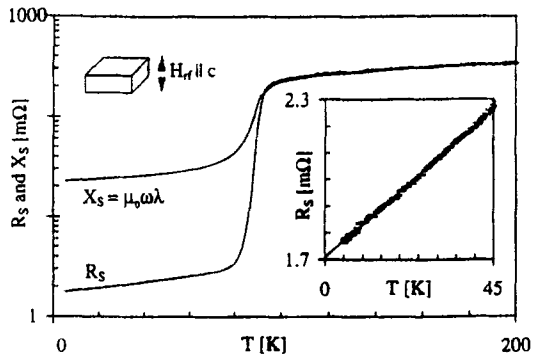

Fig. 9. Components of the surface impedance $Z_s = R_s + iX_s$ in the normal and superconducting states of a BSCCO single crystal vs. temperature [43]. The inset shows the low-temperature section of the $R_s(T)$ curve.

superconductors, the natural question arose about the applicability of properties (a) and (b) to other HTS materials which, unlike YBCO, have a tetragonal structure and contain no Cu–O chains or are copper-free. The progress in the fabrication technology of HTS samples in the past two to three years has been considerable, which has allowed researchers to investigate microwave properties of BSCCO [43,65,66], BKBO [47], TBCCO [54], and TBCO [67] single crystals of high quality. In addition, the notable reduction in the homogenization time of growth solutions and in the time of crystal growth by the conventional technique [23] of YBCO manufacture in standard zirconium dioxide (ZrO_2) crucibles stabilized with yttrium, alongside the utilization of $BaZrO_3$ crucibles [68], has allowed technologists to manufacture high-purity YBCO crystals with resistivities $\rho(T_c) < 40\ \mu\Omega \cdot$ cm, i.e., lower than in previously reported experiments. Microwave measurements of such crystals produced using the accelerated growth technique in ZrO_2 and $BaZrO_3$ crucibles have been performed recently by the ISSP [33,54] and NEU [69,70] groups. These measurements have demonstrated features (a) and (b) in the curves of $\lambda_{ab}(T)$ and $R_s(T)$, as well as new features of $Z_s(T)$ in the range of higher temperatures.

Examples of experimental curves $R_s(T)$ and $X_s(T)$ recorded in the transverse orientation, $\vec{H}_\omega \| \vec{c}$ (Fig. 5a), are given in Fig. 6 for a YBCO single crystal, in Fig. 7 for a BKBO crystal, and in Fig. 9 for a BSCCO crystal. In all these graphs, $R_s(T) = X_s(T)$ for $T \geq T_c$, which indicates that the experiments were performed under the normal skin-effect conditions. The values of $X_s(T)$ were obtained using Eq. (13), in which the additive constant X_0 was determined by fitting measurements of $\Delta X_s(T)$ to $\Delta R_s(T)$ in the range $T \geq T_c$. The quantity $X_s(T)$ expressed in absolute units, in its turn, determines $\lambda(0) = X_s(0)/\omega\mu_0$. From the measurement of

$$R_s(T_c) = \sqrt{\omega\mu_0\rho(T_c)/2} \approx 0.12\ \Omega$$

in the YBCO single crystal (Fig. 6), we derive $\rho(T_c) \approx 38\ \mu\Omega \cdot$ cm [33]. All the functions of temperature $R_s(T) = X_s(T)$ plotted in Figs. 6, 7, and 9 in the region $T \geq T_c$ are adequately described by the formula

$$2R_s^2(T)/\omega\mu_0 = \rho(T) = \rho_0 + bT$$

For example, in the BSCCO crystal (Fig. 9) $\rho_0 \approx 11\ \mu\Omega \cdot$ cm and $b \approx 1.4\ \mu\Omega \cdot$ cm/K [43].

It is more convenient to compare the surface impedance vs. temperature, $Z_s(T)$, in the superconducting state in different HTS single crystals by dividing the entire temperature interval into three sections, namely the ranges of low ($T < T_c/3$), intermediate ($T \sim T_c/2$), and subcritical ($T \sim T_c$) temperatures.

3.1. Low Temperatures, $T < T_c/3$

Figure 10 shows a set of typical $R_s(T)$ and $\lambda(T)$ curves in the range $T < 0.7T_c$ measured in YBCO [33], TBCCO [54], and BKBO [47] single crystals manufactured at ISSP. The curves for YBCO and BKBO correspond to the low-temperature sections of the graphs in Figs. 6 and 7 with the ordinate plotted using a linear scale. The experimental points of $\lambda(T)$ for YBCO are the same as those shown by open circles about curve 2 in Fig. 8.

In the low-temperature range, changes in the surface resistance, $\Delta R_s(T)$ are proportional to T for all the crystals whose data are plotted in Fig. 10. Similar linear dependences $\Delta R_s(T)$ are observed in BSCCO (inset to Fig. 9) and TBCO (Fig. 11) crystals.

The functions $\Delta\lambda(T) = \Delta X_s(T)/\omega\mu_0$ in the YBCO (Figs. 8 and 10), BSCCO (Figs. 9 and 12), and TBCO (Fig. 13) crystals in the range $T < T_c/3$ are also linear. The curves of $\lambda(T)$ for TBCCO at $T > 12$ K and for BKBO at $T > 5$ K shown in Fig. 10 have clearly rectilinear shapes.

The extrapolation of low-temperature sections of $\lambda(T)$ curves to $T = 0$ in Fig. 10 and of $X_s(T) = \omega\mu_0\lambda(T)$ in Fig. 9 yields the following estimates of $\lambda_{ab}(0)$ in several single crystals of different materials: 1400 Å (YBCO), 3700 Å (TBCCO), 3000 Å (BKBO), and 2600 Å (BSCCO).

3.2. Intermediate Temperatures, $T \sim T_c/2$

At frequencies about 10 GHz, the linear dependence $\Delta R_s(T) \propto T$ in BSCCO (Fig. 9), TBCCO (Fig.

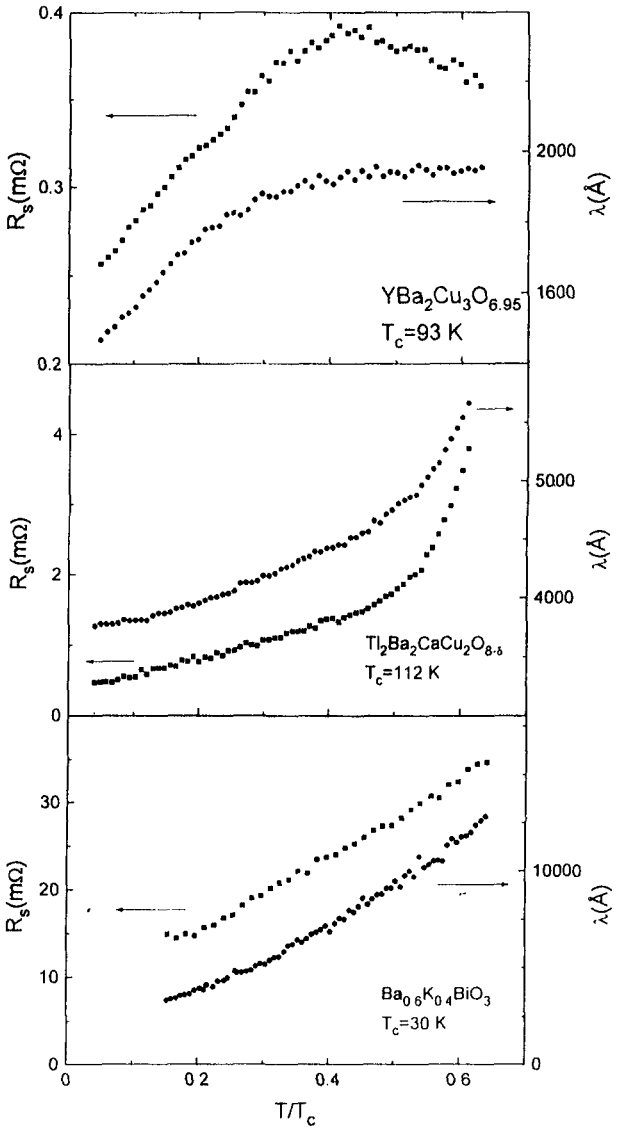

Fig. 10. Surface resistance R_s and penetration depth λ in YBCO, TBCCO, and BKBO single crystals as functions of temperature for $T<0.7T_c$.

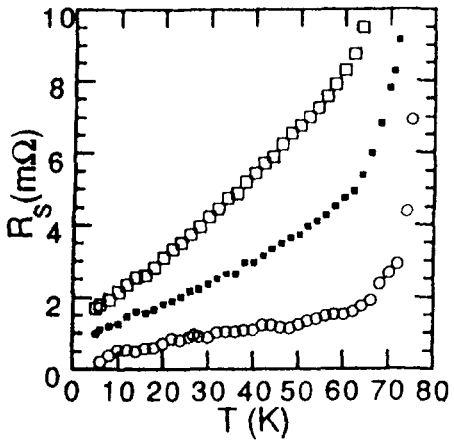

Fig. 11. Surface resistance R_s of a TBCO single crystal ($T_c \approx 78$ K) vs. temperature [67] at several frequencies: circles correspond to 14.4 GHz, black squares to 24.8 GHz, open squares to 35.9 GHz.

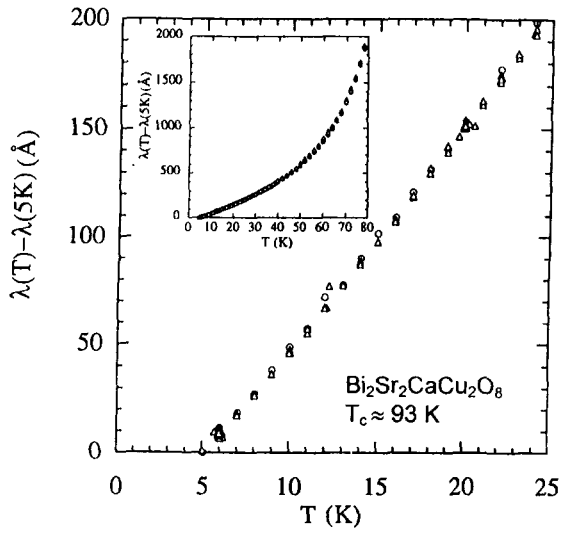

Fig. 12. Linear section of the curve of penetration depth vs. temperature, $\Delta\lambda(T)$, in a BSCCO single crystal in the low-temperature range [66]. The inset shows the curve of $\Delta\lambda(T)$ over a wider temperature range.

10), BKBO (Fig. 10), and TBCO (Fig. 11) single crystals extends to temperatures $\sim T_c/2$. The magnetic field penetration depth $\lambda(T)$ monotonically increases with the temperature.

This property of the surface impedance, common for all HTS single crystals with the tetragonal structure, is not characteristic of YBCO. As was noted previously, all microwave measurements of high-quality YBCO crystals show a broad peak in the $R_s(T)$ curve centered at about 40 K (Figs. 6 and 10). The underlying cause of this YBCO feature, which distinguishes it from other HTS materials, has remained unclear. It is unlikely that the absence of this peak in crystals with the tetragonal structure could be caused by their poor quality, as is the case of YBCO doped with Zn [57–59]. Firstly, there is a sufficiently large set of experimental data indicating that $R_s(T)$ is a linear function in BSCCO, TBCO, TBCCO, and BKBO; secondly, the peak in $R_s(T)$ was also detected in such YBCO crystals [41,54,56] whose parameters R_{res} and $\rho(T_c)$, which characterize their quality, were inferior to those of, for example, BSCCO [66] or TBCCO [54]. The more probable cause of the peak is the presence of an additional component in the YBCO orthorhombic structure, namely Cu–O chains, whose electrons form an additional electronic band

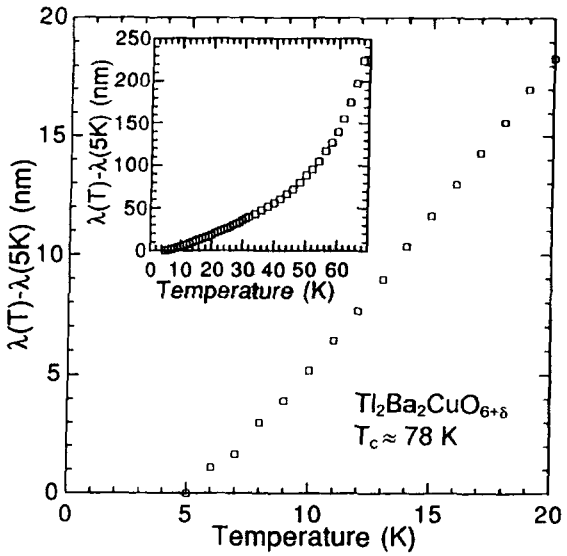

Fig. 13. Linear section of the curve of field penetration depth λ vs. temperature in a TBCO single crystal [67]. The inset shows the curve of $\Delta\lambda(T)$ over a wider temperature range.

and contribute to the function $Z_s(T)$. It seems that this contribution generates another distinctive feature of YBCO, namely the plateau (Figs. 8 and 10) or bump (Fig. 14) on the curve of $\lambda_{ab}(T)$.

This feature has been yet observed only in the purest YBCO single crystals [33,54,69,70] and films [55,71]. Curve 1 in Fig. 14 refers to a YBCO crystal with notably smaller values of $\rho(T_c)$ and R_{res} than in samples 2 and 3, whose $\Delta\lambda_{ab}(T)$ curves have a standard shape. In Figs. 6, 8, and 10 the quantities X_s and λ_{ab} are almost constant with the temperature in the intermediate range.

In discussing features of the imaginary part $X_s(T)$ of the surface impedance in the intermediate temperature range, one should be careful to take into account the possibility of crystal thermal expansion distorting the curves of $\lambda(T)$. As was shown in the previous section, this process has little effect on the shapes of the $\lambda(T)$ curves in Fig. 8. The plateaus on the $\lambda_{ab}(T)$ curves have approximately the same width of about 20 K, but their positions with respect to $T_c/2$ vary in several YBCO single crystals manufactured by the same technique [33]. Measurements on one of these crystals were performed at the laboratory under Sridhar's direction (NEU), and they confirmed the existence of a plateau. Hence, we can assert that the plateaus on the curves of $\lambda(T)$ [33,54] are real features of the surface reactance $X_s(T)$ characteristic of YBCO single crystals in the intermediate temperature range. On the other hand, the curves of surface resistance $R_s(T)$ obtained in the same experiments have the usual shape (Fig. 6).

Finally, another feature in the impedance of high-quality YBCO crystals, namely a notable

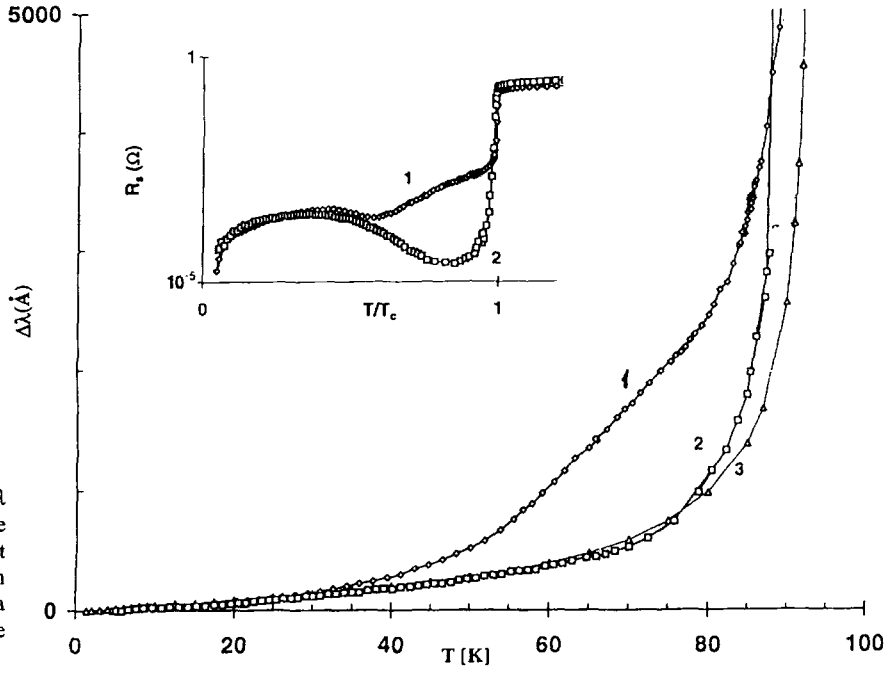

Fig. 14. Magnetic field penetration depth $\Delta\lambda$ as a function of temperature for YBCO single crystals [69] manufactured using different techniques: (1) in $BaZrO_3$ crucibles; (2) in ZrO_2 yttrium-stabilized crucibles; (3) data from [25]. The inset shows curves of surface resistance $R_s(T/T_c)$ for samples 1 and 2.

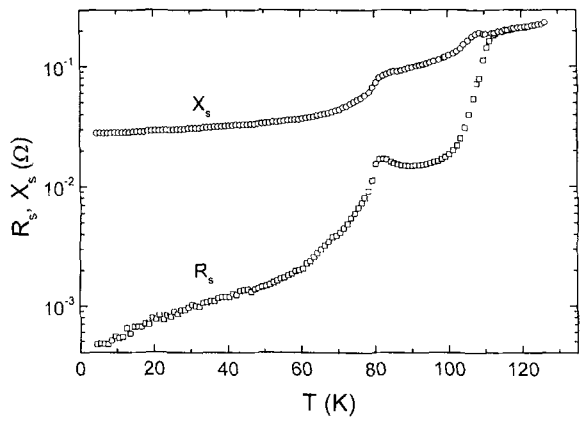

Fig. 15. Surface resistance R_s and reactance X_s of a TBCCO single crystal vs. temperature.

increase in $R_s(T)$ with temperature beyond the peak at $T \sim 40$ K, was detected in recent experiments [69,70]. The corresponding curve of $R_s(T)$ [69] is shown in the inset to Fig. 14 (curve 1). The surface resistance as a function of temperature is easily derived from measurements of the cavity Q using Eq. (13). This function is not affected by the sample thermal expansion. The gradual increase in $R_s(T)$ in the interval $T_c/2 < T < T_c$ can hardly be attributed to the coexistence of different phases in the sample. The emergence of a superconducting phase with a certain T_c is indicated in microwave experiments by a jump (an abrupt drop) in $R_s(T)$ at the critical temperature, which was observed, for example, in a TBCCO crystal (Fig. 15), which has two superconducting phases [72], namely 2212 ($T_{c1} \simeq 112$ K) and 1212 ($T_{c2} \simeq 81$ K). YBCO single crystals grown using $BaZrO_3$ crucibles and measured at a frequency of 10 GHz [69,70] are samples of record purity ($R_{res} \approx 10\ \mu\Omega$), and curve 1 in the inset to Fig. 14 proved to be reproducible [70].

3.3. Temperatures Close to T_c, $T \to T_c$

In all HTS single crystals, the surface resistance $R_s(T)$ drops abruptly at the point of transition from the normal to the superconducting state. At frequencies about 10 GHz, $R_s(T)$ of high-quality YBCO crystals falls off by a factor of 100 or more as the temperature drops to one degree below T_c. The quantity $X_s(T)$ also jumps at the transition point, but by a smaller factor. Opinions differ on the temperature dependence of the magnetic field penetration depth $\lambda_{ab}(T)$ around the critical point, which has been investigated only in YBCO crystals of high quality fabricated by different techniques. Some authors [14,73] measured the function $\lambda_{ab}(T) \propto (1 - T/T_c)^{-0.33}$, corresponding to the so-called 3D XY fluctuation model [74–76]. Others [70] detected in the neighborhood of T_c the dependence $\lambda_{ab}(T) \propto (1 - T/T_c)^{-0.5}$, in agreement with the BCS theory. The exponent measured in the crystals fabricated at ISSP proved to have an intermediate value between -0.33 and -0.5.

3.4. Complex Conductivity

Now let us discuss the temperature dependence of the complex conductivity $\sigma_s = \sigma_1 - i\sigma_2$. The components $\sigma_1(T)$ and $\sigma_2(T)$ are not measured directly but derived from measurements of $R_s(T)$ and $X_s(T)$ using Eq. (2).

At temperatures not very close to T_c and in HTS crystals of high quality $R_s(T) \ll X_s(T)$, and Eq. (2) can be simplified:

$$\sigma_1(T) = \frac{2\omega\mu_0 R_s(T)}{X_s^3(T)}, \qquad \sigma_2(T) = \frac{\omega\mu_0}{X_s^2(T)} \tag{24}$$

It follows from Eq. (24) that in the ranges of low and intermediate temperatures $\sigma_1/\sigma_2 = 2R_s/X_s \ll 1$. The increments $\Delta\sigma_1(T)$ and $\Delta\sigma_2(T)$ depend on relative changes $\Delta R_s(T)$ and $\Delta X_s(T)$:

$$\Delta\sigma_1 \propto \left(\frac{\Delta R_s}{R_s} - 3\frac{\Delta X_s}{X_s}\right), \qquad \Delta\sigma_2 \propto -\frac{\Delta X_s}{X_s} \tag{25}$$

Hence, the curves of $\sigma_2(T)$ are determined only by the function $X_s(T) = \omega\mu_0\lambda(T)$ and reflect the basic properties of the field penetration depth vs. temperature, namely its rectilinear shape at low temperatures in all high-quality HTS crystals and the features detected in YBCO in the intermediate temperature range. The behavior of the real part $\sigma_1(T)$ of the conductivity, as follows from Eq. (25), is determined by the competition between relative increments $\Delta R_s/R_s$ and $\Delta X_s/X_s$. In conventional superconductors like Nb, $X_s(T)$ ($\gg R_s$) is a very weak function of temperature in the temperature range $T \leq T_c/2$ ($\Delta X_s \approx 0$), and $R_s(T)$ drops exponentially with decreasing temperature and tends to R_{res} as $T \to 0$. By subtracting R_{res} from measurements of $R_s(T)$, we derive using Eqs. (24) and (25) the temperature dependence $\sigma_1(T)$ predicted by the BCS model: $\sigma_1 = 0$ at $T = 0$ and shows an exponentially slow growth with temperature for $T \leq T_c/2$ (Fig. 1). In HTS materials curves of $\sigma_1(T)$ are radically different from those predicted by conventional theories (BCS, SC, GC) of the microwave response of superconductors. In the range $T < T_c$ the increments $\Delta R_s(T)$ and $\Delta X_s(T)$ in HTS are not small,

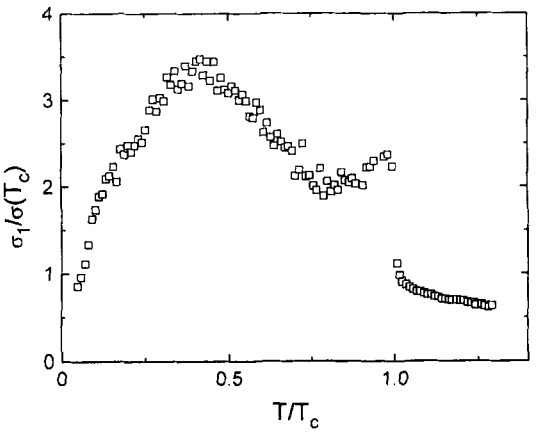

Fig. 16. Real part of the conductivity $\sigma_1(T)/\sigma(T_c)$ of a YBCO single crystal calculated by Eq. (27). Values of $R_s(T)$ substituted in this equation were derived from curves of Fig. 6 (or 10) by subtracting the residual resistance $R_{res} \simeq 230\ \mu\Omega$.

besides, $\Delta X_s(T) \gg \Delta R_s(T)$. Therefore, although $R_s(T) < X_s(T)$, the increment $\Delta\sigma_1(T)$ in Eq. (25) changes its sign from plus to minus as the temperature increases from $T=0$, i.e., the curve of $\sigma_1(T)$ should have a peak. Its position and amplitude depend on what value has been attributed to R_{res}. For this reason, the shapes of $\sigma_1(T)$ curves are not determined unambiguously for $T \leq T_c/2$, unlike the functions $R_s(T)$ and $X_s(T)$, which are directly measured in experiments. If we linearly extrapolate $R_s(T)$ to the region $T \ll T_c$ down to $T=0$ and attribute the resulting $R_s(0)$ to the residual surface resistance, $R_s(0) = R_{res}$, and then substitute the temperature-dependent difference $R_s(T) - R_{res}$ (the function due to intrinsic behavior) in the numerator of the first formula in Eq. (24), all resulting $\sigma_1(T)$ curves for HTS materials have shapes of broad peaks. Starting with a steep linear section in the neighborhood of $\sigma_1(0) = 0$, the curve of $\sigma_1(T)$ rapidly arrives at its peak value $\sigma_{1\,max}$, which is always essentially higher than the normal state conductivity $\sigma_1(T_c)$: $\sigma_{1\,max} \gg \sigma_1(T_c)$. In tetragonal HTS crystals the conductivity has its peak value $\sigma_{1\,max}$ at temperature $T_m \approx T_c/3$, and in YBCO T_m is very close to the peak position of the $R_s(T)$ curve. Moreover, the features of the YBCO surface impedance $Z_s(T)$ in the intermediate temperature range [33,54,69,70] are also manifested in the conductivity $\sigma_1(T)$ of these samples. As an example, the curve of $\sigma_1(T)$ for the YBCO crystal characterized by the curves of $R_s(T)$ and $X_s(T)$ shown in Fig. 6 is given in Fig. 16.

Let us also discuss the behavior of $\sigma_s(T)$ near T_c, where Eqs. (24) and (25) do not apply. In this temperature range, it is advisable to use local relationships (1) and (2) or their analogues for normalized quantities, relating the real and imaginary parts of the impedance to the components of complex conductivity and vice versa:

$$\frac{R_s(T)}{R_s(T_c)} \simeq \sqrt{\frac{\sigma(T_c)(\varphi^{1/2}-1)}{\sigma_2\varphi}}, \qquad (26)$$

$$\frac{X_s(T)}{X_s(T_c)} \simeq \sqrt{\frac{\sigma(T_c)(\varphi^{1/2}+1)}{\sigma_2\varphi}}$$

$$\frac{\sigma_1(T)}{\sigma(T_c)} \simeq \frac{4R_s^2(T_c)R_sX_s}{(R_s^2+X_s^2)^2}, \qquad (27)$$

$$\frac{\sigma_2(T)}{\sigma_2(0)} \simeq \frac{\lambda^2(0)}{\lambda^2(T)} \simeq \frac{X_s^2(0)(X_s^2-R_s^2)}{(R_s^2+X_s^2)^2}$$

Here $R_s(T_c) = X_s(T_c)$ and $\sigma(T_c) = \sigma_1(T_c)$ are the impedance and conductivity at $T=T_c$, $X_s(0)$ and $\sigma_2(0)$ are the values at $T=0$; $\lambda = (1/\omega\mu_0\sigma_2)^{1/2}$ and $\varphi = 1 + (\sigma_1/\sigma_2)^2$. The conductivity $\sigma_2(T)$ in the *ab*-plane of HTS crystals abruptly drops to zero in the normal state. The derivative $(T_c/\sigma_2(0))\, d\sigma_2(T)/dT$ at $T=T_c$ varies in different crystals between -2 and -4. The real part of the conductivity, $\sigma_1(T)$, does not show a coherent peak (Fig. 2) about $0.85T_c$ predicted by BCS. Usually the curve of $\sigma_1(T)$ of HTS single crystals within 1 K below T_c has the shape of a very narrow peak and transforms to a broad maximum peaking at $T < T_c/2$. The causes of the narrow peak in the close neighborhood of T_c are the inhomogeneous broadening of the superconducting transition [11,12] and fluctuation effects [13], and this peak was investigated in detail by Anlage *et al.* [14]. In very pure YBCO crystals, however, the curve of $\sigma_1(T)$ deviates from its usual shape in the range $T > T_c/2$ (Fig. 16) because of features in the impedance $Z_s(T)$ at these temperatures.

4. MODIFIED TWO-FLUID MODEL

Macroscopic properties of conventional superconductors have been successfully described by the London simple phenomenological model [77] and the related two-fluid model [17] developed by Gorter and Casimir (GC). The underlying principle of both these models is a local relation between the current density and vector potential of magnetic field. As concerns the analysis of superconductors in an electromagnetic field of frequency ω, the essence of the GC model can

be described as follows. It assumes that a superconductor contains a fraction n_s of superconducting current carriers, whereas the second fraction n_n is normal carriers (both have the same charge e and effective mass m), and at all temperatures $T \leq T_c$ the total carrier concentration is $n = n_s + n_n$. The equation of motion for the superconducting carriers is London's first equation. The normal current carriers are acted upon by an ac electric field and an averaged "force of friction," which depends on the relaxation time τ of normal carriers, and their motion is controlled by Newton's second law. By solving the equations of motion, we obtain expressions for the components of complex conductivity $\sigma_s = \sigma_1 - i\sigma_2$:

$$\sigma_1 = \frac{n_n e^2 \tau}{m} \frac{1}{1+(\omega\tau)^2}, \qquad \sigma_2 = \frac{n_s e^2}{m\omega}\left[1 + \frac{n_n}{n_s}\frac{(\omega\tau)^2}{1+(\omega\tau)^2}\right] \tag{28}$$

The relaxation time τ in the GC model is independent of temperature. This is quite natural if we assume that the behavior of normal carriers in superconductors is similar to that of normal carriers in normal metals. Scattering of electrons at low temperatures (in conventional superconductors $T_c < 10$ K) is due to impurities and independent of the temperature. Therefore the temperature dependence of the conductivity components (28) in the Gorter–Casimir model is determined by the functions $n_n(T)$ and $n_s(T) = n - n_n(T)$ only. The best agreement with experimental data is achieved if the function $n_s(t)$ is selected in the form $n_s(t) = n(1 - t^4)$, where $t = T/T_c$, which leads to the well-known formula $\lambda(t) = \lambda_L(1 - t^4)^{-1/2}$, where $\lambda_L = (m/\mu_0 n e^2)^{1/2}$. As a result, we derive from Eq. (28) $\sigma_1(T)$ and $\sigma_2(T)$, then from Eqs (1) or (26) the components of the surface impedance $R_s(T)$ and $X_s(T)$. In the band of centimeter and longer waves, the shapes of these curves weakly depend on the parameter $\omega\tau < 1$. When the temperature $T < T_c$ decreases and $\sigma_1 \ll \sigma_2$, so that, according to Eqs. (26) and (27),

$$R_s \simeq \frac{(\omega\mu_0)^{1/2}\sigma_1}{2\sigma_2^{3/2}} = \frac{1}{2}\omega^2\mu_0^2\sigma_1\lambda^3, \qquad X_s \simeq (\omega\mu_0/\sigma_2)^{1/2} = \omega\mu_0\lambda \tag{29}$$

the functions $X_s(T)/X_s(T_c)$ and $\sigma_2(T)/\sigma(T_c)$ rapidly saturate as the temperature drops and achieve their limits $(2\omega\tau)^{1/2}$ and $(\omega\tau)^{-1}$, corresponding to zero temperature, whereas $\sigma_1(T)$ and $R_s(T)$ tend to zero following a power law. In the other limiting case $(\sigma_1 \gg \sigma_2)$ of the temperature approaching T_c, $\sigma_1 \to \sigma(T_c)$, $\sigma_2 \to 0$, and the quantities

$$R_s \approx \left(\frac{\omega\mu_0}{2\sigma_1}\right)^{1/2}\left(1 - \frac{\sigma_2}{2\sigma_1}\right), \qquad X_s \approx \left(\frac{\omega\mu_0}{2\sigma_1}\right)^{1/2}\left(1 + \frac{\sigma_2}{2\sigma_1}\right) \tag{30}$$

become equal at $T = T_c$ $(t = 1)$; furthermore, there is a narrow peak of $X_s(T)$ at $t_m = (1 - \omega\tau/\sqrt{3})^{1/4}$, whose amplitude $X_s(t_m) \simeq 1.14 X_s(1)$. Such a peak has been observed in conventional superconductors tantalum and niobium [78,79].

Before proceeding with our analysis, it is advisable to compare the temperature dependences of surface impedance and complex conductivity predicted by the two-fluid GC model with those given by the microscopic BCS (Fermi liquid with weak electron–phonon coupling) and SC (strong coupling) models. General electrodynamic formulas for superconductors deriving from the BCS and SC models are given in the review [80]. One can easily derive from these formulas analytical expressions for the conductivity components in the two limiting cases of the BCS theory, which apply to dirty London and pure Pippard superconductors at frequencies $\omega \ll \Delta/\hbar$ [81,82]:

$$\frac{\sigma_1(T)}{\sigma(T_c)} \approx \frac{\Delta(T)}{2kT}\cosh^{-2}\left(\frac{\Delta}{2kT}\right)\ln\left(\frac{\Delta}{\hbar\omega}\right), \qquad \frac{\sigma_2(T)}{\sigma(T_c)} = \frac{\pi\Delta(T)}{\hbar\omega}\tanh\left(\frac{\Delta}{2kT}\right) \tag{31}$$

By comparing Eqs (31) with (28), one can easily find out that, unlike the GC model, the functions $\sigma_s(T)$ and $Z_s(T)$ given by the BCS models have the following features:

(1) in the range $T < T_c/2$ the exponential dependence ($R_s(T)$ and $\sigma_1(T) \propto \exp(-\Delta(0)/kT)$) is predominant;
(2) the slope of the $\sigma_2(T)$ curve at $T \to T_c$ is about twice as small;
(3) owing to the logarithmic factor in Eq. (31), $\sigma_1(T)$ grows in the temperature range $0.85 < T/T_c < 1$ (the coherent peak). The standard GC two-fluid model cannot account for the increase in $\sigma_1(T)$ beyond $\sigma(T_c)$, since this growth would require a number n_n of normal carriers larger than their total number n.

Nonetheless, the BCS theory allows a two-fluid interpretation in the London limit if, following Abrikosov [1], we take

$$n_n(T)=n-n_s(T)=nT^{-1}\frac{d\Delta}{dT}\left(\frac{d}{dT}\frac{\Delta}{T}\right)^{-1}$$

By substituting these functions $n_s(T)$ and $n_n(T)$ in Eq. (28), we can obtain properties (1) and (2) typical of the BCS model. The peak in $\sigma_1(T)/\sigma(T_c)$ can be obtained in the two-fluid model only by introducing an energy dependence of the relaxation time τ [83].

In the BCS there is a gap Δ, which depends only on the temperature, in the excitation spectrum at all temperatures $T<T_c$. At $T=0$ there are no quasiparticles in BCS superconductors, and the onset of the electromagnetic absorption takes place in the band of optical frequencies $\omega>2\Delta(0)/\hbar$. The energy 2Δ is necessary to break a Cooper pair and generate two excitations in a superconductor. The gap width drops with the temperature, and a lower energy $\hbar\omega$ is sufficient for generating quasiparticles through excitation across the gap. These quasiparticles are treated as a "normal liquid" in the BCS model, although they are not full analogues of current carriers in normal metals because of coherence effects related to wave functions of pairs. A more natural two-fluid description of the high-frequency response in superconductors was obtained under conditions of the SC model, as was shown in the review [84]. The distinctive feature of superconductors with strong coupling is that the gap in the spectrum of electronic excitations is smeared. Strictly speaking, there is no gap whatever at $T\neq 0$ [85,86]. This leads to breaking of Cooper pairs, smearing of the peak in the density of states, and suppression of coherence effects. If the coupling constant is sufficiently large (more than two), there is no coherent peak in the conductivity $\sigma_1(T)$, and the mechanism of quasiparticle generation is radically different from that of the BCS model [87]. They are generated without jumps across the energy gap and can be in states with all energies down to $\hbar\omega=0$. These states can be classified as gapless, and the quasiparticles can be treated as normal current carriers in the two-fluid model. Curves of $\lambda^2(0)/\lambda^2(T)$ numerically calculated by the SC model [18–20,88] proved to be fairly close to the function $n_s(t)/n=1-n_n(t)/n=1-t^4$ in the GC model. The slopes of these curves at $T=T_c$ are in agreement with those measured in different YBCO single crystals and equal to -3 [59] or -4 [33,42,54]. In combination with the experimental fact that there is no BCS coherent peak in the conductivity of HTS crystals, this indicates the necessity of taking into account effects of strong coupling near T_c and feasibility of a description of HTS properties in the high-frequency band in terms of the two-fluid model.

4.1. Temperature Dependence of the Relaxation Time

As was noted in the Introduction, none of the models briefly described in the previous sections (GC, BCS, and SC) can account for the impedance $Z_s(T)$ and conductivity $\sigma_s(T)$ as functions of temperature in the ranges of low and intermediate temperatures. There is, however, a very simple description of features detected in experiments in their entirety based on the conventional two-fluid model modified by including distinctive features of HTS materials. One of these features is the very high T_c. In normal metals, processes of inelastic scattering of quasiparticles are essential at such high temperatures, hence, one natural modification of the two-fluid model is inclusion of the temperature dependence $\tau(T)$.

The first attempts to determine this dependence by comparing measurements of $\sigma_1(T)$ and $\sigma_2(T)$ with calculations by Eq. (28) were undertaken in studying HTS crystals in which the real part of conductivity has a peak at $T\sim T_c/2$ [24,89,90]. The conclusion from this comparison was that τ should increase with decreasing temperature in the range $T<T_c$, but for some reasons (poor quality of crystals, utilization of curves measured in different experiments, etc.) the resulting functions $\tau(T)$ were rather peculiar: $1/\tau\propto\exp(T/T_0)$, $T_0\sim 10$ K [90] or $1/\tau\propto(AT^6+B)$ [89]. A more detailed analysis taking into account both common properties and specific features of the impedance and conductivity of high-quality HTS crystals was required (see the previous section), and this analysis was given in our publications [30,33,47,54,91].

The parameter $\omega\tau(T_c)$ is derived from measurements of conductivity: $\omega\tau(T_c)=\sigma_1(T_c)/\sigma_2(0)$. In the band of centimeter waves, $\omega\tau(T_c)\sim 10^{-3}$ in the best HTS crystals. There is no feasible mechanism that could lead to an increase in the relaxation time by three orders of magnitude with decreasing temperature below T_c. Therefore $\omega\tau\ll 1$ at all temperatures, and the expressions for the conductivity components in Eq. (28) in the two-fluid model transform to a very simple form:

$$\sigma_1=\frac{e^2\tau}{m}n_n,\qquad \sigma_2=\frac{e^2}{m\omega}n_s \tag{32}$$

At fixed $n_s(t)/n$, hence $n_n(t)/n = 1 - n_s(t)/n$, the only function we lack for determination of conductivity $\sigma_s(t)$ in Eq. (32) and impedance $Z_s(t)$ in Eq. (1) is $\tau(t)$.

First let us try to describe measurements of $R_s(T)/R_s(T_c)$ using Eq. (26) by substituting values of $\sigma_2(T)/\sigma_2(0) = \lambda^2(0)/\lambda^2(T) = n_s(T)/n$ measured in the same experiments and $\sigma_1(T)/\sigma_1(T_c)$ obtained using Eq. (32), the latter function, in its turn, being derived from $n_n(T)/n = 1 - \sigma_2(T)/\sigma_2(0)$, which is obtained using experimental data and properly selected $\tau(T)$.

In selecting the form of function $\tau(T)$, let us rely on the simple analogy between the "normal liquid" and charge carriers in normal metals. According to Mathissen's rule, the reciprocal relaxation time at temperatures below the Debye temperature, $T \ll \Theta$, is

$$\frac{1}{\tau} = \frac{1}{\tau_{imp}} + \frac{1}{\tau_{e\text{-}ph}} + \frac{1}{\tau_{e\text{-}e}} \tag{33}$$

The first summand on the right (due to impurity scattering) is constant with temperature, the second (electron–phonon scattering) is proportional to T^5, and the third (electron–electron scattering) is proportional to T^2. By adding the first and second summands on the right of Eq. (33), we express $\tau(T)$ as

$$\frac{1}{\tau(t)} = \frac{1}{\tau(T_c)} \frac{\beta + t^5}{\beta + 1} \approx \frac{\beta + t^5}{\tau(T_c)} \tag{34}$$

where $\beta \approx \tau(T_c)/\tau(0) \ll 1$ is a numerical parameter. Expression (34) corresponds to the low-temperature limit of the Bloch–Grünesen formula, which includes the impurity scattering and can be presented in a wide temperature range in the form

$$\frac{1}{\tau(t)} = \frac{1}{\tau(T_c)} \frac{\beta + t^5 \mathcal{J}_5(\kappa/t)\mathcal{J}_5(\kappa)}{1 + \beta},$$
$$\mathcal{J}_5(\kappa/t) = \int_0^{\kappa/t} \frac{z^5 e^z \, dz}{(e^z - 1)^2} \tag{35}$$

where $\kappa = \Theta/T_c$. For $T < \Theta/10$ ($\kappa > 10t$) Eq. (34) derives from Eq. (35); for $T > \Theta/5$ ($\kappa < 5t$) we deduce from Eq. (35) the linear dependence $1/\tau(t) \propto t$.

All experimental curves of $R_s(t)$ in high-quality YBCO single crystals can be described by the two-fluid model with $\tau(T)$ given by Eqs. (34) or (35). This is demonstrated by Fig. 17, which contains measurements labeled by A, B, and C taken from [59,33,69] and transformed to a single frequency of 10 GHz. Graph B corresponds to the curve of $R_s(T)$ in Fig. 6

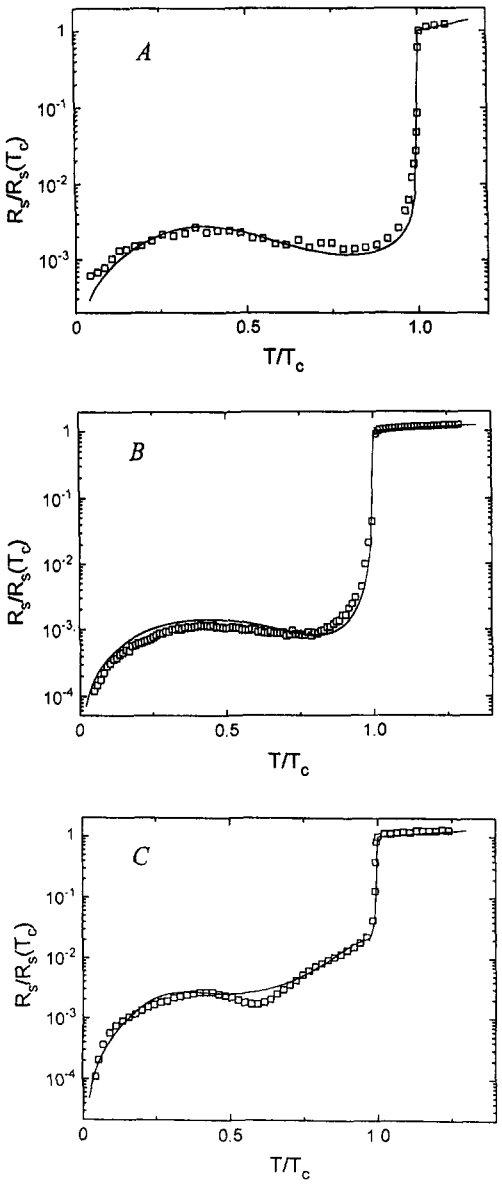

Fig. 17. Comparison between calculations (solid lines) and measurements (open squares) of surface resistance vs. temperature, $R_s(T)/R_s(T_c)$, in YBCO single crystals. Experimental data are taken from [59] (A, 4.13 GHz), [33] (B, 9.42 GHz), and [69] (C, 10 GHz) and transformed ($\propto \omega^{3/2}$) to one frequency 10 GHz.

and graph C to curve 1 in the inset to Fig. 14. At this frequency $\omega\tau(T_c) = [\rho(T_c)\sigma_2(0)]^{-1}$ proved to be approximately $4 \cdot 10^{-3}$, i.e., in these experiments [33,59,69] $1/\tau(T_c) \approx 2 \cdot 10^{13}$ s^{-1}. The solid lines in Fig. 17 show calculations of $R_s(T)/R_s(T_c)$ by Eqs (26) and (32) with $\sigma_2(T)/\sigma_2(0)$ derived from the same experimental data [59,33,69] and plotted in Fig. 20

(curves A–C). Curve A in Fig. 17 was plotted using only one fitting parameter $\beta = 0.01$ in Eq. (34). For curve B $\beta = 0.2$ in Eq. (34), and for curve C $\beta = 0.02$ and $\kappa = 4$ in Eq. (35). The calculated curves are very close to experimental data and display both common and specific features of $R_s(T)$ of YBCO crystals fabricated by different methods, namely, the broad peak in the intermediate temperature range due to the fast growth of the relaxation time, $\tau(T) \propto T^{-5}$, with decreasing temperature and the increase in $R_s(T)$ in the range $T_c/2 < T < T_c$ (curve C) [69] caused by the crossover from T^{-5} to T^{-1} in Eq. (35) for $\tau(T)$, which occurs in this sample (C) at temperatures lower than in samples A and B. Hence follows the conclusion that the shape of the $R_s(T)$ curve in YBCO single crystals is controlled mostly by the phonon scattering of quasiparticles.

Figure 18 shows an experimental curve of $R_s(T)$ plotted in linear coordinates [59], which was measured in the same sample as curve A in Fig. 17, but at a higher frequency, where the value $\omega\tau(T_c) \approx 1.5 \cdot 10^{-2}$ was used in calculations (solid curve). The dashed and dash-dotted curves in Fig. 18 also plot $R_s(T)/R_s(T_c)$, but these data were calculated by replacing the temperature dependence of $1/\tau(t)$ in Eq. (34) proportional to t^5 with t^2 for the former, whereas in the latter case τ was assumed to be constant with temperature. We stress once again that the peak in $R_s(T)$ typical of YBCO at $T \sim 0.4T_c$ can be described only using the dependence $1/\tau(t) \propto t^5$. In addition, only this function leads to a

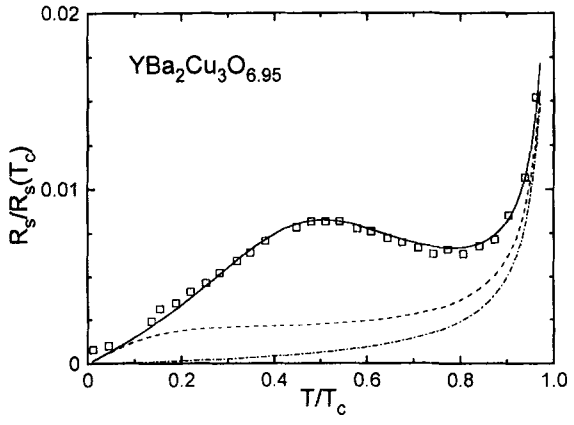

Fig. 18. Open squares plot experimental data for a YBCO single crystal [59] at a frequency of 34.8 GHz; lines are calculations by Eq. (26). The dashed line was calculated with summand t^5 replaced by t^2 in the numerator of Eq. (34), the dash-dotted line with the temperature dependence eliminated from Eq. (34).

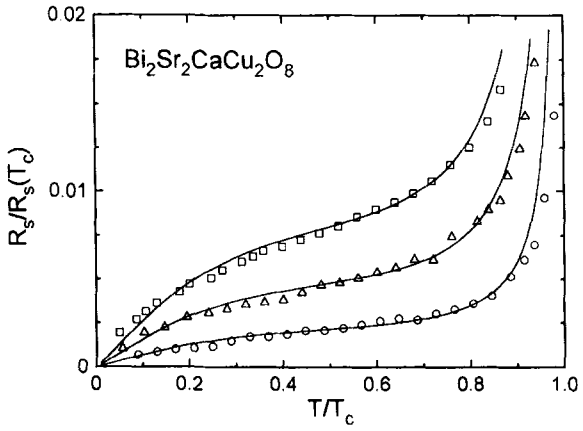

Fig. 19. Experimental data for a BSCCO single crystal [66] obtained at different frequencies: circles plot measurements at 14.4 GHz, triangles at 24.6 GHz, and squares at 34.7 GHz. Solid lines are calculations of $R_s(T)/R_s(T_c)$ at the frequencies given above.

notable elevation of $R_s(T)$ curves in a wide temperature range, which is a common feature of all HTS materials.

The inclusion of the third summand on the right of Eq. (33), i.e., a term quadratic in temperature in the numerator in Eq. (34), leads to spreading of the peak. This proves essential in comparing model curves with measurements of tetragonal HTS crystals, which, unlike YBCO, do not show a peak in $R_s(T)$. In Fig. 19 the symbols plot experimental data obtained by Lee *et al.* [66] in a BSCCO crystal at three frequencies: 14.4 GHz ($\omega\tau(T_c) = 0.8 \cdot 10^{-2}$), 24.6 GHz, and 34.7 GHz. The solid lines shows calculations at these frequencies by Eqs. (26) and (32) using measurements of $\sigma_2(T)/\sigma_2(0) = n_s(T)/n$ in the same experiments [66] and the function

$$\frac{1}{\tau(t)} = \frac{\beta + \gamma t^2 + t^5}{\tau(T_c)(\beta + \gamma + 1)} \tag{36}$$

where $\beta = 0.1$ and $\gamma = 0.9$.

Graphs of Figs. 17–19, which plot measurements of different crystals at different frequencies, demonstrate excellent agreement between experimental data on $R_s(T)$ and calculations based on the two-fluid model.

4.2. Temperature Dependence of the Superconducting Electron Density

Now let us try to analyze directly measurements of $\sigma_2(T)/\sigma_2(0)$. Figure 20A shows a curve of $\lambda^2(0)/\lambda^2(t) = n_s(t)/n$ in the *ab*-plane of a YBCO crystal [59].

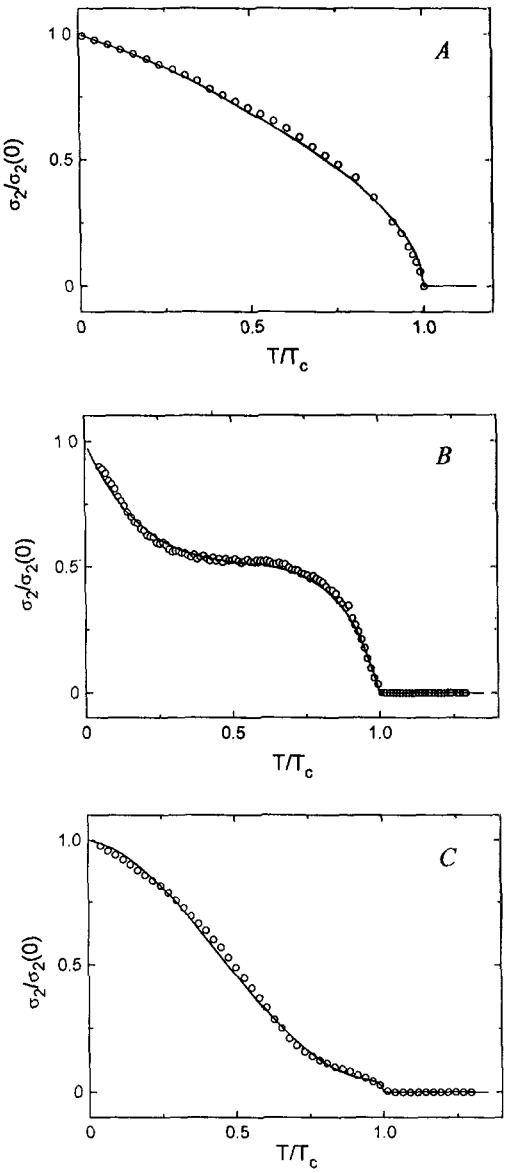

Fig. 20. Comparison between calculations (solid lines) and measurements (circles) of $\sigma_2(T)/\sigma_2(0)=\lambda^2(0)/\lambda^2(T)$ for YBCO single crystals. Experimental data are taken from [59] (A), [33] (B), and [69] (C).

Similar curves with small variations in their slopes at low temperatures and in the neighborhood of T_c were obtained in other experiments with both YBCO [42,56], and tetragonal BSCCO [43,66] and TBCO [67] crystals. All of them are characterized by linear sections in the low-temperature range and well approximated by the function

$$n_s/n=(1-t)^{\alpha} \tag{37}$$

where α is a numerical parameter. For $t\ll 1$ we have $n_s(t)/n=\sigma_2(t)/\sigma_2(0)\simeq(1-\alpha t)$. In the experiments quoted here $0.5\leq\alpha\leq 0.7$. The solid lines in Fig. 20A show function (37) at $\alpha=0.5$. Near T_c we obtain $\lambda(t)\propto n_s(t)^{-1/2}\propto(1-t)^{-\alpha/2}$, which is also in fairly good agreement with experimental data. Equation (37) yields an infinite value of derivative $d\sigma_2(t)/dt\propto(1-t)^{\alpha-1}$ at $t=1$ and $\alpha<1$.

The function $n_s(t)$, however, cannot account in its simplest form (37) for features in the curves of $\lambda^2(0)/\lambda^2(T)$ detected recently in YBCO crystals in the intermediate temperature range [33,54,69,70]. Moreover, the slope of these curves at $T\ll T_c$ implies that $\alpha>1$ in Eq. (37), which would lead to zero slope of the $\sigma_2(T)/\sigma_2(0)$ curve at $T=T_c$. Therefore we have to introduce an additional summand to the right-hand side of Eq. (37) without breaking the condition of particle conservation, $n_s+n_n=n$, in the two-fluid model:

$$n_s/n=(1-t)^{\alpha}(1-\delta)+\delta(1-t^{4/\delta}) \tag{38}$$

where $0<\delta<1$ is the weight factor. For $\delta\ll 1$ ($\delta\to 0$) and $\alpha>1$ the principal contribution to $\sigma_2(T)$ throughout the temperature range is still due to the first term on the right of Eq. (38), whereas the second is responsible for the finite slope of $\sigma_2(T)/\sigma_2(0)$ at $T=T_c$ equal to -4, in accordance with the GC model. As δ increases, the second term on the right of Eq. (38) becomes more significant. The experimental curve of $\sigma_2(T)/\sigma_2(0)$ in Fig. 20B derived from $R_s(T)$ and $X_s(T)$ and plotted in Fig. 6 using formula (27) is adequately described by function (38) at $\delta=0.5$ and $\alpha=5.5$. The curve plotting this function in Fig. 20B reflects characteristic features of the experimental data, namely, the linear section and positive second derivative ($a>1$) in the low-temperature range, the plateau in the intermediate temperature range due to the equality ($\delta=0.5$) between the summands in Eq. (38), and the correct value of the slope near T_c. The whole set of $\sigma_2(T)$ curves measured in the *ab*-plane of YBCO crystals grown at ISSP using the same technique is described by Eq. (38), where α was almost constant, $\alpha\approx 5.5$, and δ was varied between 0.1 and 0.5.

The third curve in Fig. 20C [69], which corresponds to the curve of $\lambda(T)$ in Fig. 14 (1), is different from typical curves of Figs. 20A and 14 (2), (3), since a linear section of $\sigma_2(T)$ is observed only in a narrow range of temperatures, $0<T\ll T_c$, and it switches to a quadratic curve as the temperature increases. This crossover can be described [33] by introducing an additional factor $(1+\eta t)$ to the first summand on the right of Eq. (38) for $n_s(t)$; thus we can obtain the solid curve of Fig. 20C at $\alpha=2.2$, $\eta=2$, and $\delta=0.04$.

To sum up, one can describe characteristic features of $Z_s(T)$ and $\sigma_s(T)$ in high-quality HTS crystals in terms of the modified two-fluid model based on Eqs. (32)–(38). As follows from these equations, at low temperatures, $t \ll 1$, all curves have linear sections, $\sigma_1 \propto \alpha t/\beta$, since $n_n/n \approx \alpha t$ and $\tau \approx \tau(0) \approx \tau(T_c)/\beta$; $\Delta\sigma_2 \propto -\alpha t$; $R_s \propto \alpha t/\beta$, in accordance with Eq. (29); $\Delta X_s \propto \Delta\lambda \propto \alpha t/2$. As the temperature increases, the curve of $\sigma_1(t)$ passes through a maximum at $t < 0.5$. This peak is due to superposition of two competing effects, namely, the drop in the number of normal carriers as the temperature decreases, $t < 1$, and the increase in the relaxation time, which stalls at $t \sim \beta^{1/5}$. The model also accounts for the temperature dependence of the surface impedance and complex conductivity in YBCO single crystals manufactured using different techniques.

5. ON THE WAY TO A MICROSCOPIC THEORY

Let us set aside the feasible mechanisms of superconducting pairing in HTS and briefly analyze the existing microscopic theories of the high-frequency response of HTS materials. Given the phenomenological model formulated in the previous section, which is in fairly good agreement with measurements of $Z_s(T)$ in HTS crystals, it is natural to compare the tenets of this model with results of the microscopic theory. Along the way, some progress toward a clear understanding of a universal microscopic approach to microwave properties of HTS may be possible.

5.1. Isotropic SC Model and Relaxation Time in the Superconducting State

Eliashberg's equations, which take into account effects of delay and damping of quasiparticles, apply to superconductors with an arbitrarily strong interaction in the Fermi liquid. In the case of electron–phonon interaction in an isotropic one-band superconductor with singlet s-wave pairing and Debye spectrum of phonons, the electron relaxation rate $\Gamma(T) = 1/2\tau(T)$ is proportional to T^3 for $T < T_c$ [16,84] if Eliashberg's equations are solved by neglecting the phonon corrections to the electromagnetic vertex. If these corrections are taken into account [92], then $\Gamma(T) \propto T^5$, which is in agreement with Eq. (34). Using this result, the authors of [15] proved that peaks on curves of $R_s(T)$ and $\sigma_1(T)$, which are characteristic features of YBCO, can be obtained on the base of the conventional isotropic SC model, although quantitative agreement between this model and experimental data is out of the question. To the best of our knowledge, the theory suggested by Eliashberg *et al.* [92] has remained the only model applied to the HTS microwave response taking into account vertex corrections. It might be interesting to find out whether this result [92] should hold in microscopic models more adequate for description of HTS.

5.2. Model of Almost Antiferromagnetic Fermi Liquid

In this model [93–95], low-frequency excitations in the medium are not phonons, but weakly damped spin waves, and superconducting pairing is mediated by spin fluctuations. The paramagnon mechanism leads to a d-wave symmetry of the order parameter, when the Fermi surface contains lines on which the gap width turns to zero. This means that there are quasiparticles in the superconductor even at $T = 0$, hence the finite conductivity [96]

$$\sigma_{\min} = \frac{ne^2}{m\pi\Delta_0} = \frac{2\Gamma(T_c)\sigma(T_c)}{\pi\Delta_0} \tag{39}$$

Here $2\Gamma(T_c) = 1/\tau(T_c)$, and Δ_0 is the maximum gap width on the Fermi surface, $\Delta_0 = 2.14T_c$ (hereafter $\hbar = k = 1$) if strong coupling effects are neglected. Recall that $2\Gamma(T_c) = 2 \cdot 10^{13}\ \mathrm{s}^{-1} \simeq 0.8T_c$ for YBCO single crystals [33,59,69]; then we derive from Eq. (39) $\sigma_{\min} \simeq 0.1\sigma(T_c)$, and substitution of this parameter in Eq. (29) yields the minimum surface resistance $R_{s\,\min}$ of a d-wave superconductor. At a frequency of 10 GHz in YBCO $R_{s\,\min} \sim 1\ \mu\Omega$, i.e., one order of magnitude lower than the best experimental data reported to date.

These manifestations of the d-wave symmetry, which are unusual from the viewpoint of the conventional approach, stimulated theoretical studies of various HTS properties based on the model of an almost antiferromagnetic Fermi liquid.

Hirschfeld *et al.* [97–99] calculated the conductivity $\sigma_s(T)$ and surface resistance $R_s(T)$ as functions of temperature and compared them to experimental data by Bonn *et al.* [59]. Let us discuss these results in detail.

First let us consider the case of relatively low temperatures $T < 0.4T_c$, when the quasiparticle damping is due to their impurity scattering. In this range, as was indicated by Hirschfeld *et al.* [97–99],

(1) the integral expressions for the superconductor microwave response allow one to present the conductivity in the form of Eqs (28) or (32) with

$\tau(T) \approx \tau(0) \equiv 1/2\Gamma$, where Γ is the rate of elastic relaxation; Γ is always smaller than $\Gamma(T_c)$; for example, in the experiment by Bonn *et al.* [59], $\Gamma/\Gamma(T_c) \simeq \tau(T_c)/\tau(5\text{ K}) \simeq \beta \approx 0.01$;

(2) versions with weak (Born approximation) and strong (unitary limit) scattering characterized by phase shifts $\delta = 0$ and $\delta = \pi/2$, respectively, are considered; in the Born approximation suppression of T_c is predicted but has not been detected in microwave experiments;

(3) there is a crossover temperature T^* defining the boundary between the "gapless" ($T < T^* \ll T_c$) and "pure" ($T^* < T \ll T_c$) regimes of superconductivity; in the unitary limit, whose conditions are closer to those of real experiments, $T^* \approx 0.8(\Gamma\Delta_0)^{1/2} \approx 0.1T_c \simeq 9$ K in the best YBCO crystals with optimal doping level; introduction of impurities (such as Zn [59]) leads to higher Γ and crossover temperature T^*.

In the "pure" regime of superconductivity the field penetration depth is a linear function of nondimensional temperature $t = T/T_c$:

$$\frac{\lambda(t)}{\lambda(0)} = 1 + c_1 t, \qquad c_1 = \frac{T_c \ln 2}{\Delta_0} \tag{40}$$

This formula is in agreement with Eq. (37), from which follows

$$\frac{\lambda(t)}{\lambda(0)} = 1 + \alpha t/2, \qquad t \ll 1 \tag{41}$$

By taking $\alpha = 0.5$ (for the curve in Fig. 20A) and $2c_1$ given in Eq. (40), we obtain $\Delta_0 \simeq 2.7T_c$ in the experiment reported by Bonn *et al.* [59]. At frequencies of 4 GHz ($\omega/T_c \simeq 0.002$) and 35 GHz ($\omega/T_c \simeq 0.019$) the parameter ω/Γ in [59] equals $0.2T_c$ and $1.9T_c$, respectively, which corresponds to an intermediate region between the hydrodynamic ($\omega/\Gamma \ll 1$) and collisionless ($\omega/\Gamma \gg 1$) limits. According to numerical calculations [98,99] for this intermediate region (measurements at 35 GHz in [59] are well within this region), the conductivity $\sigma_1(T)$ is a linear function of T. Figure 9 in [99] clearly shows that the slope of the line describing $\sigma_1(T)/\sigma(T_c)$ at $T \ll T_c$ is close to α/β, which is given by the phenomenological model.

As the concentration of impurities increases, the "pure" regime at low temperatures is replaced by the "gapless" one, and from the intermediate region the system is shifted to the hydrodynamic one; as a result, we have $\Delta\lambda(T) \propto T^2$ and $\sigma_1(T) \propto T^2$. This conclusion was confirmed by measurements [59] of samples with Cu atoms substituted by Zn impurities.

In the temperature range $T > 0.4T_c$ processes of inelastic scattering are significant. The quasiparticle damping factor due to scattering by spin fluctuations vs. temperature was calculated neglecting vertex corrections [100], and the result was proportional to T^3: $1/\tau(T) \propto T^3$. With due account of this formula, calculations in the range of intermediate temperatures and in the neighborhood of T_c produced maxima on curves of $\sigma_1(T)$ and $R_s(T)$ [98,99]. Unfortunately, the parameter $\Gamma/T_c = 0.0008$ used in those calculations was undervalued; therefore, it was useless to compare these calculations with accurate experimental data. One remarkable fact revealed by this comparison was that the peak in the calculated $R_s(T)$ was shifted to lower temperatures with respect to the measured position, which might be caused by the insufficiently strong temperature dependence of $1/\tau$ in the calculations (compare with Fig. 18).

Thus, the *d*-wave model of the microwave response [97–99] is in qualitative agreement with measurements of surface impedance in YBCO at low temperatures [59] and is consistent from the formal viewpoint with the phenomenological model considered above at $T \ll T_c$. A significant advantage of these calculations [97–99] is the visual demonstration of nontrivial consequences of the *d*-wave order parameter applied to investigations of microwave response of high-quality YBCO single crystals using the minimal number of fitting parameters. It seems that curves of $\sigma_2(T)$ measured in tetragonal HTS crystals, like those shown in Fig. 20A, can also be described by this model. On the other hand, this model cannot account for the linear section of the $R_s(T)$ curves extending to $T_c/2$ (at a frequency of 10 GHz), observation of radically different values of the $\sigma_2(T)$ slope for $T \ll T_c$ (which corresponds to $\alpha > 1$ in Eq. (38) and, in accordance with Eq. (40), to $\Delta_0 < T_c$) in experiments with YBCO crystals [33,54,69,70], not to mention features in the range of intermediate temperatures, and, finally, the large slopes of $R_s(T)$ and $\sigma_2(T)$ curves as $T \to T_c$.

This approach was further developed in a recent work by Hensen *et al.* [71], who compared in detail calculations and measurements of $Z_s(T)$ at a frequency of 87 GHz in two different YBCO films. They investigated theoretically the evolution of functions $\sigma_s(T)$ and $R_s(T)$ as a result of a transition from the unitary to the Born limit and demonstrated that the minimal conductivity in Eq. (39) is not a universal parameter and the experimental curves are best described at an intermediate scattering phase shift $\delta \approx 0.4\pi$. They matched their calculations to the

experimental data using a combination of six (or even nine) fitting parameters. Three parameters were contained in a phenomenologically introduced temperature dependence of the inelastic relaxation time $\tau(1)/\tau(t) = at^3 + (1-a)\, e^{b_1(t-1)[1+b_2(t-1)^2]}$, where $t = T/T_c$. In the case of film B with higher characteristics [71], the parameter $a = 0$, and the remaining terms are well approximated by the function $1/\tau(T) \propto T^5$. It is desirable to apply this calculation technique [71] and its version generalized to the case of strong coupling [101] to measurements of HTS crystals in the centimeter wavelength band.

To conclude our discussion of the consequences of the *d*-wave order parameter, which is due to the interaction intensity described by an alternating function in the reciprocal space, consider two important points. Firstly, the presence of quasi-one-dimensional sections of the electronic spectrum in HTS and the resulting square-root van Hove singularities in the density of states [102] lead to the *d*-wave pairing caused by anisotropic electron–phonon coupling. Alternative models of the *d*-wave order parameter based on the electron–phonon coupling were discussed in [103,104]. Secondly, the third principle of thermodynamics rules out the linear dependence $\Delta\lambda(T) \propto T$ in the region of very low temperatures, $T \to 0$ [105]. In the case of a superconductor with a *d*-wave order parameter, this means that there always exists a physical mechanism that gives rise to a crossover temperature $T^* \ll T_c$ below which $\Delta\lambda(T)$ must deviate from a linear function. At present two such mechanisms are known, namely the impurity scattering [97] and, in pure *d*-wave superconductors, nonlocal effects [2]. Indeed, in some microwave experiments the onset of the linear section of the $\Delta\lambda(T)$ curve in the range $T \ll T_c$ was not at 4.2 K, but at slightly higher temperatures (see, for example, curves of $\lambda(T)$ in TBCCO and BKBO shown in Fig. 10), but no systematic measurements of $\Delta\lambda(T)$ for $T < 5$ K are presently available.

5.3. Two-Band Model and Mixed Symmetry of the Order Parameter

An interpretation of the features in $Z_s(T)$ and $\sigma_s(T)$ curves observed recently in YBCO single crystals [33,54,69,70] can be based on the two-band model and/or the assumption about the mixed symmetry of the order parameter. Even the shapes of the experimental curves in Figs. 20B and C, and function (38), which describes these curves and contains two summands, provide evidence in favor of this interpretation. Moreover, the mixed $(s+d)$-wave order parameter has the symmetry of the orthorhombic lattice and seems to be more natural for YBCO than a pure *d*-wave order parameter, which has the symmetry of the tetragonal lattice.

A description of HTS properties based on the two-band model was suggested by Kresin and Wolf [106]. This model is a generalization of the SC model to the case of layered HTS, in particular YBCO, which has two subsystems, namely the band of CuO_2 planes (*S*-band) and the band of CuO chains (*N*-band). The density of states in such a system as a function of temperature and impurity concentration was analyzed by Adrian *et al.* [107].

Calculations of the microwave response [22,108,109] assumed a strong electron–phonon coupling in the *S*-band and a weak superconductivity in the *N*-band induced by the proximity effect. A system of coupled Eliashberg equations for the *s*-wave order parameter and renormalization functions in each band was solved. The parameters in these equations were coupling constants λ_{ij} and coefficients γ_{ij} and γ_{ij}^M of scattering from the *i*th to the *j*th band due to nonmagnetic and magnetic impurities, respectively.

In [22,109] the number and values of parameters were selected using experimental data on YBCO single crystals. For the *S*-band $\lambda_{11} = 3$, in the *N*-band $\lambda_{22} = 0$, and the nonvanishing gap in the CuO chains is induced by the interband coupling characterized by the parameters $\lambda_{12} = \lambda_{21} = 0.2$. This set of coupling constants yields $T_c \simeq 92$ K. Effects of interband scattering were considered to be negligible: $\gamma_{12}, \gamma_{21} \ll T_c$. Impurity scattering within each band, γ_{11}, γ_{22}, was taken into account, alongside the scattering by magnetic impurities, $\gamma_{22}^M \equiv \gamma^M$, in the *N*-band only ($\gamma_{11}^M = 0$), where oxygen atoms have a higher mobility and, leaving the chains, generate magnetic moments in the uncompensated copper ions Cu^{2+}. The parameter γ^M is proportional to the concentration of the magnetic impurities, which increases with decreasing oxygen content in the sample. The constants of elastic relaxation were considered to be equal, $\gamma_{11} = \gamma_{22} = \gamma^{\text{imp}}$, and estimated taking the absolute value and anisotropy of YBCO conductivity in the normal state, namely, the estimate $2 \le \gamma^{\text{imp}}/T_c \le 4$ derived from the measurement $50 < \rho(100\text{ K}) \le 100\ \mu\Omega \cdot \text{cm}$ and the resistivity anisotropy factor in the *ab*-plane equal to 2. Note that γ^{imp} is not equal to $\Gamma = 1/2\tau(0)$ in the one-band models discussed above. The calculated constants of inelastic scattering were automatically proportional to T^3 [22,109], since the Debye phonon spectrum was used and vertex corrections were neglected. Thus the large set of parameters initially included

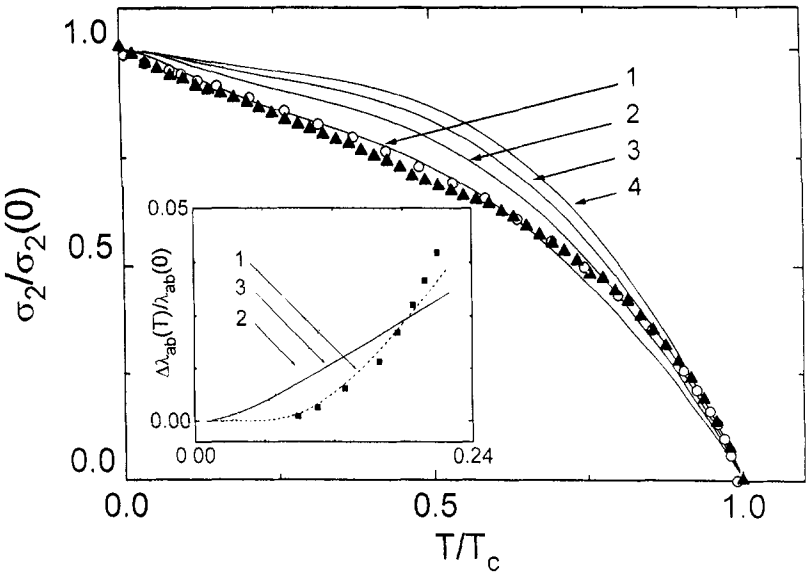

Fig. 21. Comparison between calculated curves ($\gamma^M = 0.2T_c$) of $\sigma_2(T)/\sigma_2(0)$ and experimental data from [42] (triangles) and [59] (circles): (1) $\gamma^{imp} = 2T_c$; (2) $\gamma^{imp} = 4T_c$; (3) $\gamma^{imp} = 8T_c$; (4) $\gamma^{imp} = 20T_c$. The inset ($\gamma^{imp} = 2T_c$) demonstrates a crossover from the exponential (curves 1, $\gamma^M = 0$, and 2, $\gamma^M = 0.1T_c$) to linear (curve 3, $\gamma^M = 0.4T_c$) curve of $\Delta\lambda_{ab}(T)$ due to increasing concentration of magnetic impurities. Squares in the inset plot data from [55].

in the Eliashberg equations for the two-band model reduced to four numbers λ_{11}, λ_{12}, γ^{imp}, and γ^M, two of which ($\lambda_{11} = 3$ and $\lambda_{12} = 0.2$) were constant, whereas γ^{imp} and γ^M varied.

Figure 21 shows calculations and measurements given in [42] and [59] (Fig. 20A) of the function $\sigma_2(T)/\sigma_2(0)$. For curves (1–4) $\gamma^M = 0.2T_c = \text{const}$, and the only parameter varying from one curve to another is γ^{imp}: $2T_c$ (1), $4T_c$ (2), $8T_c$ (3), and $20T_c$ (4). The effect of magnetic impurity scattering (depending on the content of oxygen in YBCO) is demonstrated by the inset to Fig. 21 and can be described as follows. In a sample saturated with oxygen, there are no magnetic scatterers in the chains (N-band), $\gamma^M = 0$. In this case, the calculation by the two-band model (curve 1 in the inset) and the experimental data (■) obtained using a YBCO thin film [55] yield an exponential temperature dependence $\Delta\lambda_{ab}(T)$ for $T \ll T_c$, owing to the small width of the energy gap induced in the N-band.

Note that an exponential dependence $\Delta\lambda(T)$ has been detected by now in only one experiment [55] with YBCO films of very high quality, which degraded very rapidly [110]. No such behavior has been observed in the best HTS crystals. The thermally activated behavior of $\sigma_s(T)$ and $R_s(T)$ is incompatible with the d-wave symmetry of the order parameter.

Light doping with magnetic impurities ($\gamma^M = 0.1T_c$, curve 2 in the inset to Fig. 21) leads to a large slope of $\Delta\lambda_{ab}(T)$, but does not radically change the curve shape. A further increase in γ^M (depletion of oxygen) makes the superconducting state in the chains gapless, and the function $\Delta\lambda_{ab}(T)$ becomes linear in the temperature range $T > 0.05T_c \approx 5$ K. A linear section of the $\Delta\lambda_{ab}(T)$ curve in the low temperature range is also shown in Fig. 3, where the curve calculated on the basis of the model under discussion ($\gamma^M = 0.3T_c$, $\gamma^{imp} = 4T_c$) is compared to measurements of a YBCO thin film at a frequency of 87 GHz [21]. At a sufficiently high γ^{imp}, the contribution of the N-band to the field penetration depth vanishes, and the function $\Delta\lambda(T)$ becomes close to that predicted by the SC model: $\Delta\lambda(T) \propto T^n$ with the exponent $n > 2$ [16,92]. A crossover from a linear $\Delta\lambda(T)$ to a power function with $n = 4$ with increasing impurity concentration was observed in recent experiments [111] with YBCO crystals with some Y atoms replaced by Pr ions.

The complex conductivity $\sigma_s = \sigma_1 - i\sigma_2$ of a two-band superconductor is a combination of conductivities in the S-band ($\sigma_s^S = \sigma_1^S - i\sigma_2^S$) and N-band ($\sigma_s^N = \sigma_1^N - i\sigma_2^N$):

$$\sigma_s = \sigma_s^S + \zeta\sigma_s^N, \qquad \zeta = \frac{\nu^S m^N}{\nu^N m^S} \tag{42}$$

where $\nu^{S,N}$ and $m^{S,N}$ are the densities of states and effective masses of carriers in the respective bands. Numerical calculations of $\sigma_1(T)$ and $R_s(T)$ [109] are in satisfactory agreement with measurements of YBCO films [21], although these data have not been carefully analyzed as yet in the range of low temperatures and near T_c.

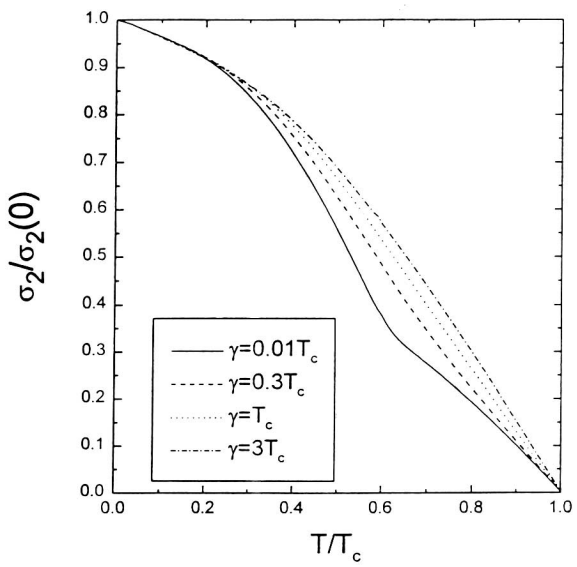

Fig. 22. Evolution of $\sigma_2(T)/\sigma_2(0)$ curves due to changes in the interband scattering constant γ. Calculations are made by the two-band model with a d-wave order parameter in the S-band and an s-wave order parameter in the N-band [112].

Even though the two-band model has its uncontested advantages, attempts to apply it to the microwave response of tetragonal HTS single crystals is problematic since, unlike YBCO, they contain no chains and, therefore, no magnetic scatterers like Cu^{2+} ions in YBCO. Meanwhile, magnetic impurities play an essential role: scattering by these impurities reduces the gap in the N-band to zero and leads to the linear temperature dependence of $\Delta\lambda_{ab}$ for $T \ll T_c$. There is no such problem with d-wave superconductors. Moreover, it seems that the experimental curves of $Z_s(T)$ and $\sigma_s(T)$ in YBCO in the intermediate temperature range cannot be interpreted in terms of s-pairing in both bands. Therefore, an option with a d-wave order parameter in one of the bands turns up as a matter of course. An attempt to introduce such an order parameter was made by Golubov, and calculations of $\sigma_2(T)/\sigma_2(0)$ are plotted in Fig. 22 [112]. The curves were calculated using a two-band model with a d-wave superconducting gap in the S-band and s-wave symmetry in the N-band. The model parameters were $\lambda_{11}=3$, $\lambda_{22}=0.5$, in Eq. (42) $\zeta=0.5$, and only the constants of interband scattering $\gamma_{12}=\gamma_{21}\equiv\gamma$ were included. The solid line in Fig. 22 shows a feature at $T\approx 0.6T_c$, which vanishes as the disorder increases. A similar approach was employed by Srikanth *et al.* [70] in interpreting their experimental data, in particular, for the phenomenological description of the curve in Fig. 20C. Recently the microwave properties of HTS materials have been attracting more attention from researchers [113–117] because of intriguing effects that are tentatively attributed to the mixed $(s+d)$-wave symmetry of the order parameter, and more interesting discoveries in this field of research can be expected in the immediate future.

6. CONCLUSION

This review is an attempt to summarize and classify measurements of the surface impedance $Z_s(T)=R_s(T)+iX_s(T)$ of high-quality YBCO, BKBO, TBCCO, TBCO, and BSCCO crystals in the temperature range $4.2\leq T\leq 150$ K. The common features of all these materials are the linear temperature dependence of surface resistance, $\Delta R_s(T)\propto T$, and reactance, $\Delta X_s(T)\propto\Delta\lambda_{ab}(T)\propto T$, at temperatures $T\ll T_c$, their rapid growth as $T\to T_c$, and their behavior in the normal state corresponding to the linear dependence $\Delta\rho_{ab}(T)\propto T$, $R_s(T)=X_s(T)=\sqrt{\omega\mu_0\rho(T)/2}$. There are differences between the curves of $Z_s(T)$ in BSCCO, TBCCO, and TBCO single crystals with tetragonal lattices, and BKBO crystals with the cubic lattice on one hand, and YBCO crystals with the orthorhombic structure on the other. Whereas the linear sections of these curve in the tetragonal materials, $\Delta R_s(T)\propto T$, obtained at a frequency of $\sim$10 GHz can extend to $T_c/2$, in YBCO the linear section terminates at $T<T_c/3$, and at higher temperature the $R_s(T)$ curve has a broad peak. In addition, the $\lambda_{ab}(T)$ curves of YBCO have features in the intermediate temperature range.

The paper suggests a simple description of all these properties of $Z_s(T)$ based on the two-fluid model, which takes into account scattering of quasiparticles and characteristic changes in the density of superconducting carriers at low temperatures and in the neighborhood of the critical temperature. The underlying ideas of this model may be essential for a future microscopic model of the microwave response of HTS materials.

Only microwave properties of HTS crystals of the highest quality and with optimal doping levels have been discussed, because a great deal of experimental data concerning these materials has been accumulated by this time. For this reason, we have set aside three issues, which are, in our opinion, quite important and worth mentioning at the end of the review.

Firstly, the evolution of the temperature dependence $Z_s(T)$ with changes in the doping level from the optimal value has not been studied sufficiently. No

microwave measurements of one and the same crystal but with a variable and controlled carrier concentration are available. At the same time, such data are essential for theoretical studies aimed at creating a microscopic theory of HTS, because they will shed light on such problems as possible changes in the order parameter symmetry [118,119], evolution of the pseudogap [120–122], superconductor–dielectric transitions [123], etc.

Secondly, the nature of the residual surface resistance of HTS crystals measured in experiments remains unclear. The effect of the sample surface conditions on the $Z_s(T)$ signal has not been studied, although there are several phenomenological [124–130] and microscopic [131–136] models indicating the importance of such studies. For example, the theory [136] predicts that in the case of diffuse scattering on the surface, an *s*-wave component can be added to the bulk *d*-wave order parameter in the region near the sample surface. Probably, this effect can be responsible for the difference among curves of $\sigma_2(T)$ in Fig. 20 measured in YBCO with approximately equal parameters characterizing their quality. Recent microwave experiments [137] also indicate that studies of microscopic properties of single-crystal surfaces are important.

Thirdly, measurements of the surface impedance anisotropy, which remain scarce up to now, have not been discussed, although several experiments have provided evidence in favor of different temperature dependences of the surface impedance in the *ab*-plane and along the *c*-axis [41–43,45,65]. The theory [22,109,128–143] predicts different scenarios for processes in HTS in the microwave band, depending on the mechanism responsible for the anisotropy; therefore a comparison between theoretical data and accurate microwave measurements would, undoubtedly, be very helpful.

Presently solutions to the problems listed above are in the pipeline, and it seems that they will determine the development of experimental and theoretical research of the microwave response of HTS materials in the immediate future.

ACKNOWLEDGMENTS

I am grateful to my co-authors and colleagues A. A. Zhukov, A. A. Golubov, A. T. Sokolov, O. V. Dolgov, G. E. Tsydynzhapov, S. V. Shul'ga, L. A. Klinkova, N. V. Barkovskii, G. A. Emel'chenko, I. G. Naumenko, and N. N. Kolesnikov for their help and contribution to this work at different stages. Helpful discussions with V. F. Gantmakher, E. G. Maksimov, D. V. Shovkun, and G. M. Eliashberg are also acknowledged.

This research was supported by the Russian Fund for Basic Research (grant 97-02-16836) and the Scientific Council on Superconductivity (project 96060), and in part by the Program for Russian–Dutch Research Cooperation (NWO).

REFERENCES

1. A. A. Abrikosov, *Fundamentals of the Theory of Metals* (Elsevier, Amsterdam, 1988).
2. I. Kosztin and A. J. Leggett, *Phys. Rev. Lett.* **79**, 135 (1997).
3. J. Bardeen, L. N. Cooper, and J. R. Schrieffer, *Phys. Rev.* **108**, 1175 (1957).
4. A. A. Abrikosov, L. P. Gor'kov, and I. M. Khalatnikov, *Zh. Exp. Teor. Fiz.* **35**, 265 (1958) [*Sov. Phys. JETP* **8**, 182 (1959)].
5. D. C. Mattis and J. Bardeen, *Phys. Rev.* **111**, 412 (1958).
6. J. P. Turneaure, J. Halbritter, and H. A. Schwettman, *J. Supercond.* **4**, 341 (1991).
7. O. Klein, E. J. Nicol, K. Holczer, and G. Grüner, *Phys. Rev. B* **50**, 6307 (1994).
8. M. R. Trunin, A. A. Zhukov, and A. T. Sokolov, *Zh. Exp. Teor. Fiz.* **111**, 696 (1997) [*Sov. Phys. JETP* **84**, 383 (1997)].
9. G. M. Eliashberg, *Zh. Exp. Teor. Fiz.* **38**, 966 (1960) [*Sov. Phys. JETP* **11**, 696 (1960)].
10. F. Marsiglio, *Phys. Rev. B* **44**, 5373 (1991).
11. H. K. Olsson and R. H. Koch, *Phys. Rev. Lett.* **68**, 2406 (1992).
12. A. A. Golubov, M. R. Trunin, S. V. Shulga, D. Wehler, J. Dreibholz, G. Müller, and H. Piel, *Physica C* **213**, 139 (1993).
13. M. L. Horbach, W. van Saarlos, and D. A. Huse, *Phys. Rev. Lett.* **67**, 3464 (1991).
14. S. M. Anlage, J. Mao, J. C. Booth, D. H. Wu, and J. L. Peng, *Phys. Rev. B* **53**, 2792 (1996).
15. O. V. Dolgov, E. G. Maksimov, A. E. Karakozov, and A. A. Mikhailovsky, *Solid State Commun.* **89**, 827 (1994).
16. G. V. Klimovich, A. V. Rylyakov, and G. M. Eliashberg, *Pis'ma Zh. Exp. Teor. Fiz.* **53**, 381 (1991) [*JETP Lett.* **53**, 399 (1991)].
17. C. S. Gorter and H. Casimir, *Phys. Z.* **35**, 963 (1934).
18. A. A. Mikhailovsky, S. V. Shulga, A. E. Karakozov, O. V. Dolgov, and E. G. Maksimov, *Solid State Commun.* **80**, 511 (1991).
19. R. T. Collins, Z. Schlesinger, F. Holtzberg, C. Field, U. Welp, G. W. Crabtree, J. Z. Liu, and Y. Fang, *Phys. Rev. B* **43**, 3701 (1991).
20. J. Rammer, *Europhys. Lett.* **5**, 77 (1991).
21. S. Orbach-Werbig, A. A. Golubov, S. Hensen, G. Müller, and H. Piel, *Physica C* **235–240**, 2383 (1994).
22. A. A. Golubov, M. R. Trunin, A. A. Zhukov, O. V. Dolgov, and S. V. Shulga, *Pis'ma Zh. Exp. Teor. Fiz.* **62**, 477 (1995) [*JETP Lett.* **62**, 496 (1995)].
23. R. Liang, P. Dosanjh, D. A. Bonn, D. J. Baar, J. F. Carolan, and W. N. Hardy, *Physica C* **195**, 51 (1992).
24. D. A. Bonn, P. Dosanjh, R. Liang, and W. N. Hardy, *Phys. Rev. Lett.* **68**, 2390 (1992).
25. W. N. Hardy, D. A. Bonn, D. C. Morgan, R. Liang, and K. Zhang, *Phys. Rev. Lett.* **70**, 3999 (1993).
26. S. Sridhar and W. L. Kennedy, *Rev. Sci. Instrum.* **54**, 531 (1988).
27. J. Mao and S. Anlage, *Theory of Surface Impedance of Superconductors in a Resonant Cavity*, unpublished.
28. T. Shibauchi, A. Maeda, H. Kitano, T. Honda, and K. Uchinokura, *Physica C* **203**, 315 (1992).

29. O. Klein, S. Donovan, M. Dressel, and G. Grüner, *Int. J. Infrared Millimeter Waves* **14**, 2423 (1993); *ibid.*, 2459, 2489.
30. M. R. Trunin, *Usp. Fiz. Nauk*, **168** (1998).
31. J. L. Altman, *Microwave Circuits* (Van Nostrand, Princeton, 1964).
32. N. N. Kolesnikov, M. P. Kulakov, Yu. A. Osipyan, and S. A. Shevchenko, *Sverkhprovodimost': Fiz., Khim., Tekh.* **4**, 957 (1991).
33. M. R. Trunin, A. A. Zhukov, G. A. Emel'chenko, and I. G. Naumenko, *Pis'ma Zh. Exp. Teor. Fiz.* **65**, 893 (1997) [*JETP Lett.* **65**, 938 (1997)].
34. L. D. Landau and E. M. Lifschitz, *Electrodynamics of Continuous Media* (Pergamon, Oxford, 1984).
35. V. N. Trofimov, A. V. Kuznetsov, P. V. Lepeshkin, K. A. Bolshinskov, A. A. Ivanov, and A. A. Mikhailov, *Physica C* **183**, 135 (1991).
36. G. E. Gough and N. J. Exon, *Phys. Rev. B* **50**, 488 (1994).
37. M. Benkraouda and J. R. Clem, *Phys. Rev. B* **53**, 5716 (1996).
38. E. Zeldov, A. I. Larkin, V. B. Geshkenbein, M. Konczykowski, D. Majer, B. Khaykovich, V. M. Vinokur, and H. Shtrikman, *Phys. Rev. Lett.* **73**, 1428 (1994).
39. M. V. Indenbom and E. H. Brandt, *Phys. Rev. Lett.* **73**, 1731 (1994).
40. C. P. Poole, Jr., *Electron Spin Resonance: A Comprehensive Treatise on Experimental Techniques* (Interscience, New York, 1967).
41. H. Kitano, T. Shibauchi, K. Uchinokura, A. Maeda, H. Asaoka, and H. Takei, *Phys. Rev. B* **51**, 1401 (1995).
42. J. Mao, D. H. Wu, J. L. Peng, R. L. Greene, and S. M. Anlage, *Phys. Rev. B* **51**, 3316 (1995).
43. T. Jacobs, S. Sridhar, Q. Li, G. D. Gu, and N. Koshizuka, *Phys. Rev. Lett.* **75**, 4516 (1995).
44. K. Zhang, D. A. Bonn, S. Kamal, R. Liang, D. J. Baar, W. N. Hardy, F. Basov, and T. Timusk, *Phys. Rev. Lett.* **73**, 2484 (1994).
45. A. Hosseini, S. Kamal, D. A. Bonn, R. Liang, and W. N. Hardy, cond-mat/9803272.
46. L. A. Klinkova, N. V. Barkovskii, S. A. Zver'kov, and D. A. Gusev, *Sverkhprovodimost': Fiz., Khim., Tekh.* **7**, 1437 (1994).
47. M. R. Trunin, A. A. Zhukov, G. E. Tsydynzhapov, A. T. Sokolov, L. A. Klinkova, and N. V. Barkovskii, *Pis'ma Zh. Exp. Teor. Fiz.* **64**, 783 (1996) [*JETP Lett.* **64**, 832 (1997)].
48. H. You, J. D. Axe, X. B. Kan, S. Hashimoto, S. C. Moss, J. Z. Liu, G. W. Crabtree, and D. J. Lam, *Phys. Rev. B* **38**, 9213 (1988).
49. C. Meingast, B. Blank, H. Bürkle, B. Obst, T. Wolf, H. Wühl, V. Selvamanickam, and K. Salama, *Phys. Rev. B* **41**, 11299 (1990).
50. C. Meingast, O. Kraut, T. Wolf, H. Wühl, A. Erb, and G. Müller-Vogt, *Phys. Rev. Lett.* **67**, 1634 (1991).
51. H. Kierspel, H. Winkelmann, T. Auweiler, W. Schlabitz, B. Büchner, V. H. M. Duijn, N. T. Hein, A. A. Menovsky, and J. J. M. Franse, *Physica C* **262**, 177 (1996).
52. C. Meingast, A. Junod, and E. Walker, *Physica C* **272**, 106 (1996).
53. N. V. Anshukova, Yu. V. Boguslavskii, A. I. Golovashkin, L. I. Ivanova, I. B. Krynetskii, and A. P. Rusakov, *Fiz. Tverd. Tela* **35**, 1415 (1993).
54. A. A. Zhukov, M. R. Trunin, A. T. Sokolov, and N. N. Kolesnikov, *Zh. Exp. Teor. Fiz.* **112**, 2210 (1997) [*Sov. Phys. JETP* **85**, 1211 (1997)].
55. N. Klein, N. Tellmann, H. Schulz, K. Urban, S. A. Wolf, and V. Z. Kresin, *Phys. Rev. Lett.* **71**, 3355 (1993).
56. T. Jacobs, S. Sridhar, C. T. Rieck, K. Scharnberg, T. Wolf, and J. Halbritter, *J. Phys. Chem. Solids* **56**, 1945 (1995).
57. D. Achir, M. Poirier, D. A. Bonn, R. Liang, and W. N. Hardy, *Phys. Rev. B* **48**, 13184 (1993).
58. K. Zhang, D. A. Bonn, R. Liang, D. J. Baar, and W. N. Hardy, *Appl. Phys. Lett.* **62**, 3019 (1993).
59. D. A. Bonn, S. Kamal, K. Zhang, R. Liang, D. J. Baar, E. Klein, and W. N. Hardy, *Phys. Rev. B* **50**, 4051 (1994).
60. J. F. Annett, N. D. Goldenfeld, and S. R. Renn, *Phys. Rev. B* **43**, 2778 (1991).
61. Z. Ma, R. C. Taber, L. W. Lombardo, A. Kapitulnik, M. R. Beasley, P. Merchant, C. B. Eom, S. Y. Hou, and J. M. Phillips, *Phys. Rev. Lett.* **71**, 781 (1993).
62. A. Porch, M. J. Lancaster, and R. G. Humphries, *IEEE Trans. Microwave Theor. Tech.* **43**, 306 (1995).
63. L. A. de Vaulchier, J. P. Vieren, Y. Guldner, N. Bontemps, R. Combescot, Y. Lemaitre, and J. C. Mage, *Europhys. Lett.* **33**, 153 (1996).
64. D. A. Bonn and W. N. Hardy, in *Physical Properties of High-Temperature Superconductors V*, D. M. Ginsberg, ed. (World Scientific, Singapore, 1995), pp. 7–97.
65. T. Shibauchi, N. Katase, T. Tamegai, and K. Uchinokura, *Physica C* **264**, 227 (1996).
66. S-F. Lee, D. C. Morgan, R. J. Ormeno, D. M. Broun, R. A. Doyle, and J. R. Waldram, *Phys. Rev. Lett.* **77**, 735 (1996).
67. D. M. Broun, D. C. Morgan, R. J. Ormeno, S. F. Lee, A. W. Tyler, A. P. Mackenzie, and J. R. Waldram, *Phys. Rev. B* **56**, R11443 (1997).
68. A. Erb, E. Walker, and R. Flükiger, *Physica C* **258**, 9 (1996).
69. H. Srikanth, B. A. Willemsen, T. Jacobs, S. Sridhar, A. Erb, E. Walker, and R. Flükiger, *Phys. Rev. B* **55**, R14733 (1997).
70. H. Srikanth, Z. Zhai, S. Sridhar, A. Erb, and E. Walker, *Phys. Rev. B* **57**, 7986 (1998).
71. S. Hensen, G. Müller, C. T. Rieck, and K. Scharnberg, *Phys. Rev. B* **56**, 6237 (1997).
72. V. S. Simonov and V. N. Molchanov, *Kristallografiya* **41**, 31 (1996).
73. S. Kamal, D. A. Bonn, N. Goldenfeld, P. J. Hirschfeld, R. Liang, and W. N. Hardy, *Phys. Rev. Lett.* **73**, 1845 (1994).
74. C. J. Lobb, *Phys. Rev. B* **36**, 3930 (1987).
75. D. S. Fisher, M. P. A. Fisher, and D. A. Huse, *Phys. Rev. B* **43**, 130 (1991).
76. M. B. Salamon, J. Shi, N. Overend, and M. A. Howson, *Phys. Rev. B* **47**, 5520 (1993).
77. F. London and H. London, *Proc. Roy. Soc. London* **A149**, 71 (1935).
78. C. Varmazis, J. R. Hook, D. J. Sandiford, and M. Strongin, *Phys. Rev. B* **11**, 3354 (1975).
79. C. Varmazis, Y. Imry, and M. Strongin, *Phys. Rev. B* **13**, 2880 (1976).
80. S. B. Nam, *Phys. Rev.* **156**, 470, 487 (1967).
81. E. M. Lifshitz and L. P. Pitaevskii, *Physical Kinetics* (Pergamon, Oxford, 1981).
82. M. Tinkham, *Introduction to Superconductivity* (McGraw-Hill, New York, 1975).
83. J. R. Waldram, P. Theopistou, A. Porch, and H.-M. Cheah, *Phys. Rev. B* **55**, 3222 (1997).
84. V. L. Ginzburg and E. G. Maksimov, *Sverkhprovodimost': Fiz., Khim., Tekh.* **5**, 1543 (1992).
85. G. M. Eliashberg, *Zh. Exp. Teor. Fiz.* **39**, 1437 (1960) [*Sov. Phys. JETP* **12**, 1000 (1961)].
86. A. E. Karakozov, E. G. Maksimov, and S. A. Mashkov, *Zh. Exp. Teor. Fiz.* **68**, 1937 (1975) [*Sov. Phys. JETP* **41**, 971 (1976)].
87. A. E. Karakozov, E. G. Maksimov, and A. A. Mikhailovskii, *Zh. Exp. Teor. Fiz.* **102**, 132 (1992) [*Sov. Phys. JETP* **75**, 70 (1992)].
88. A. Andreone, C. Cantoni, A. Cassinese, A. Di Chiara, and R. Vaglio, *Phys. Rev. B* **56**, 7874 (1997).
89. T. Shibauchi, A. Maeda, H. Kitano, T. Honda, and K. Uchinokura, *Physica C* **203**, 315 (1992).
90. D. A. Bonn, R. Liang, T. M. Riseman, D. J. Baar, D. C. Morgan, K. Zhang, P. Dosanjh, T. L. Duty, A. MacFarlane, G. D. Morris, J. H. Brewer, W. N. Hardy, C. Kallin, and A. J. Berlinsky, *Phys. Rev. B* **47**, 11314 (1993).

91. M. R. Trunin, A. A. Zhukov, and A. T. Sokolov, *J. Phys. Chem. Solids* (1998).
92. G. M. Eliashberg, G. V. Klimovich, and A. V. Rylyakov, *J. Supercond.* **4**, 393 (1991).
93. A. Millis, H. Monien, and D. Pines, *Phys. Rev. B* **42**, 167 (1990).
94. H. Monien, P. Monthoux, and D. Pines, *Phys. Rev. B* **43**, 275 (1991).
95. P. Monthoux, A. Balatsky, and D. Pines, *Phys. Rev. B* **46**, 14803 (1992).
96. P. A. Lee, *Phys. Rev. Lett.* **71**, 1887 (1993).
97. P. J. Hirschfeld and N. Goldenfeld, *Phys. Rev. B* **48**, 4219 (1993).
98. P. J. Hirschfeld, W. O. Putikka, and D. J. Scalapino, *Phys. Rev. Lett.* **71**, 3705 (1993).
99. P. J. Hirschfeld, W. O. Putikka, and D. J. Scalapino, *Phys. Rev. B* **50**, 4051 (1994).
100. S. M. Quinlan, D. J. Scalapino, and N. Bulut, *Phys. Rev. B* **49**, 1470 (1994).
101. A. Bille and K. Scharnberg, *J. Phys. Chem. Solids* (1998).
102. *A. A. Abrikosov, Physica C* **214**, 107 (1993); **222**, 191 (1994); **244**, 243 (1995).
103. G. Santi, T. Jarlborg, M. Peter, and M. Weger, *Physica C* **259**, 253 (1996).
104. H. Kamimura, S. Matsuno, Y. Suwa, and H. Ushio, *Phys. Rev. Lett.* **77**, 723 (1996).
105. N. Schopohl and O. V. Dolgov, *Phys. Rev. Lett.* **80**, 4761 (1998).
106. V. Z. Kresin and S. A. Wolf, *Phys. Rev. B* **41**, 4278 (1990); **46**, 6458 (1992); **51**, 1229 (1995).
107. S. D. Adrian, S. A. Wolf, O. Dolgov, S. Shulga, and V. Z. Kresin, *Phys. Rev. B* **56**, 7878 (1997).
108. S. D. Adrian, M. E. Reeves, S. A. Wolf, and V. Z. Kresin, *Phys. Rev. B* **51**, 6800 (1995).
109. A. A. Golubov, M. R. Trunin, A. A. Zhukov, O. V. Dolgov, and S. V. Shulga, *J. Phys. I France* **6**, 2275 (1996).
110. M. Hein, in *Studies of High-Temperature Superconductors*, A. Narlikar, ed. (Nova Sciences, New York, 1996), Vol. 18, pp. 141–216.
111. H. Srikanth, S. Sridhar, D. A. Gajewski, and M. B. Maple, *Physica C* **291**, 235 (1997).
112. A. A. Golubov, unpublished.
113. R. Combescot and X. Leyronas, *Phys. Rev. Lett.* **75**, 3732 (1995).
114. C. O'Donovan and J. P. Carbotte, *Phys. Rev. B* **52**, 4568 (1995); **55**, 8520 (1997).
115. H. Kim and E. J. Nicol, *Phys. Rev. B* **52**, 13576 (1995).
116. S. V. Pokrovsky and V. L. Pokrovsky, *Phys. Rev. B* **54**, 13275 (1996).
117. R. Modre, I. Schürrer, and E. Schachinger, *Phys. Rev. B* **57**, 5496 (1998).
118. V. M. Loktev, *Fiz. Nizk. Temp.* **22**, 3 (1996).
119. E. A. Pashitskii and V. I. Pentegov, *Zh. Exp. Teor. Fiz.* **111**, 298 (1997) [*Sov. Phys. JETP* **84**, 164 (1997)].
120. Yu. A. Izyumov, *Usp. Fiz. Nauk* **167**, 465 (1997).
121. S. G. Ovchinnikov, *Usp. Fiz. Nauk* **167**, 1043 (1997).
122. X.-G. Wen and P. A. Lee, *Phys. Rev. Lett.* **80**, 2193 (1998).
123. V. F. Gantmakher, L. P. Kozeeva, A. N. Lavrov, D. A. Pushin, D. V. Shovkun, and G. E. Tsydynzhapov, *Pis'ma Zh. Exp. Teor. Fiz.* **65**, 834 (1997) [*JETP Lett.* **65**, 870 (1997)].
124. J. Halbritter, *J. Supercond.* **5**, 171, 331 (1992); **8**, 691 (1995).
125. A. M. Portis, in *Electrodynamics of High-Temperature Superconductors*, Lecture Notes in Physics (World Scientific, Singapore, 1993), Vol. 48.
126. O. G. Vendik and A. Yu. Popov, *Philos. Mag. Lett.* **65**, 219 (1992).
127. M. Mahel, *Solid State Commun.* **97**, 209 (1996).
128. A. V. Velichko, N. T. Cherpak, E. V. Izhyk, A. Ya. Kirichenko, and I. N. Chukanova, *Physica C* **277**, 101 (1997).
129. J. McDonald and J. R. Clem, *Phys. Rev. B* **56**, 14723 (1997).
130. T. Jacobs, K. Numssen, R. Schwab, R. Heidinger, and J. Halbritter, *IEEE Trans. Appl. Supercond.* **7**, 1917 (1997).
131. M. Matsumoto and H. Shiba, *J. Phys. Soc. Jpn.* **64**, 3384 (1995).
132. Y. Tanaka and S. Kashiwaya, *Phys. Rev. Lett.* **74**, 3451 (1996); *Phys. Rev. B* **53**, 11957 (1996).
133. S. R. Bahkal, *Phys. Rev. Lett.* **76**, 3634 (1996).
134. Yu. S. Barash, A. A. Svidzinsky, and H. Burkhardt, *Phys. Rev. B* **55**, 15282 (1997).
135. M. Fogelström, D. Rainer, and J. A. Sauls, *Phys. Rev. Lett.* **79**, 281 (1997).
136. A. A. Golubov and M. Yu. Kupriyanov, *Pis'ma Zh. Exp. Teor. Fiz.* **67**, 478 (1998) [*JETP Lett.* **67**, 499 (1998)].
137. S. Kamal, R. Liang, A. Hosseini, D. A. Bonn, and W. N. Hardy, cond-mat/9803292.
138. R. A. Klemm and S. H. Liu, *Phys. Rev. Lett.* **74**, 2343 (1995).
139. W. A. Atkinson and J. P. Carbotte, *Phys. Rev. B* **52**, 10601 (1995); **55**, 12748 (1997).
140. A. A. Abrikosov, *Physica C* **258**, 53 (1996).
141. R. J. Radtke, V. N. Kostur, and K. Levin, *Phys. Rev. B* **53**, R522 (1996).
142. T. Xiang and J. M. Wheatley, *Phys. Rev. Lett.* **76**, 134 (1996); **77**, 4632 (1996).
143. P. J. Hirschfeld, S. M. Quinlan, and D. J. Scalapino, *Phys. Rev. B* **55**, 12742 (1997).